Stability of the Theta Method for Systems with Multiple Time-Delayed Variables

Andreas Bouterakos[a], Georgios Tzounas[a]*

School of Electrical and Electronic Engineering, University College Dublin, Ireland

*Corresponding author.

E-mail address: georgios.tzounas@ucd.ie

Abstract The paper focuses on the numerical stability and accuracy of implicit time-domain integration (TDI) methods when applied for the solution of a power system model impacted by time delays. Such a model is generally formulated as a set of delay differential algebraic equations (DDAEs) in non index-1 Hessenberg form. In particular, the paper shows that numerically stable ordinary differential equation (ODE) methods, such as the trapezoidal and the Theta method, can become numerically unstable when applied to a power system that includes a significant number of delayed variables. Analysis reveals how numerical stability is primarily governed by the number of delayed variables and the strength of their Jacobian coefficients, whereas the influence of the delay magnitudes themselves is found to be comparatively minor. Numerical stability is examined through a scalar test delay differential equation, as well as through a matrix pencil approach that accounts for the DDAEs of any given dynamic power system model. Simulation results are presented in a case study based on the IEEE 39-bus system, as well as the real-world scale model of the All-Island Irish Transmission System (AIITS).

Keywords: Time-domain simulation, time delays, Theta method, numerical stability, matrix pencils.

1 Introduction

1.1 Motivation

The most successful to date approach to study the dynamic response and performance of a power system following a large disturbance is to perform nonlinear time-domain simulations. The focus of this paper is on how time-domain simulations are impacted in the presence of time delays, in particular how the numerical stability and accuracy of state-of-the-art time-domain integration (TDI) methods can be challenged in the presence of multiple time-delayed variables.

Time delays are inherent to many control systems, as measurement acquisition, data transmission, and actuation each require a certain amount of time. In conventional power systems, measurement and communication delays in local and wide-area control loops are known to degrade dynamic performance. The topic is also becoming increasingly relevant with the growing number of inverter-based DERs, which gives rise to more points of control and coordination, and thus to more data that need to be processed and transferred. As a result, the total number of control signals in the system impacted by delays is also

increasing significantly. In many cases, these delays cannot be neglected, as they may pose a threat to the overall system security, e.g., see [1–7]. While the presence and effects of delays have been widely discussed in both control and power-system literature, the numerical implications of such delays on state-of-art time-domain integration methods used in power system software tools remain largely unexplored.

1.2 Literature Review

Power system models for short-term stability analysis are conventionally described by a set of nonlinear differential algebraic equations (DAEs) [8]. These equations are known to be *stiff*, as their time constants span multiple time scales. To deal with system stiffness and ensure numerical stability, an implicit ordinary differential equation (ODE) method, such as the trapezoidal or the Theta method [9–11], is typically employed when conducting a TDI of a power system model.

Inclusion of time delays leads to the reformulation of the power system model into a set of delay differential algebraic equations (DDAEs). A common approach to handle these delays in TDI is through modification of standard ODE numerical methods [12, 13]. Nevertheless, the numerical stability properties of ODE methods do not transfer to time-delayed systems [14, 15]. For example, it is known that no A-stable natural Runge–Kutta method is stable on the whole class of stable linear systems of delay differential equations [16]. Alternatively, more sophisticated, specialized methods for delay systems can be employed at an additional computational cost, e.g., we cite the family of Radau IIA methods [17].

Selecting a proper TDI method is generally a matter of finding a good trade-off between numerical stability, precision and computational speed. In this context, the classical approach to test the stability properties of a TDI method is by studying its response when applied to a linear scalar equation representing the class to which the examined system belongs, e.g., see [18]. This approach neglects the dynamics of the specific model examined and thus is not suitable for precision assessment. Precision is typically estimated through truncation error analysis [19]. However, such an analysis is insufficient to predict numerical instabilities. Aiming to address the limitations of these approaches, the second author of this paper has recently proposed a matrix pencil approach that allows studying numerical stability and precision of TDI methods in a unified way. Such an approach was first formulated for DAE models in [20], where numerical errors between power system dynamics and the dynamics of the discrete-time system that arise due to the application of the TDI method were investigated through a comparison of their associated matrix pencils. A further investigation was carried out in [21], where participation factor analysis was used to assess the numerical deformation that standard TDI methods introduce to the shape of the coupling between dynamic modes and system variables.

The focus of the present work is on the numerical stability and accuracy of standard implicit TDI methods when employed for the numerical solution of DDAE power system models. In this vein, a preliminary study using the matrix pencil approach was carried out in [22]. Therein, results indicate

that, including a delay that is multiple of the time step in a single variable does not have a notable effect on numerical stability. In this paper, we build upon previous work to provide new theoretical insights and studies suggesting that the number of time-delayed variables and the magnitudes of their coefficients in the DDAEs are crucial factors impacting both numerical stability and accuracy and can lead otherwise very robust implicit methods to behave poorly.

1.3 Contributions

The novel contributions of this paper are as follows. We provide a first comprehensive discussion on how standard implicit TDI methods, such as the trapezoidal and Theta method, can become unstable when applied to power system models impacted by multiple time-delayed variables. In particular, we show that the main drivers of numerical instability are the number of delayed variables and the strength of their Jacobian coefficients in the system, whereas the delay magnitude itself is found to play rather a minor role. A proof of concept is first provided through a linear test delay differential equation. Then, a systematic analysis that accounts for the dynamics of real-world power system models is carried out through proper extension of a matrix pencil approach recently proposed by the second author. Time delays which are not multiples of the time step are duly taken into account. The potential of compensating numerical instabilities through simple adjustments of the damping parameter of the Theta method is also duly discussed.

1.4 Paper Organization

The remainder of the paper is organized as follows. Section 2 recalls the formulation and numerical integration of DDAE power system models. The proposed numerical stability analysis is presented in Section 3. Section 4 discusses the case study. The case study first considers the standard IEEE 39-bus system and then a modified version of the same system that includes inverter-based distributed energy resources (DERs). Conclusions are drawn in Section 5.

2 Numerical Integration in the Presence of Delays

2.1 Conventional DAE Model

Power system dynamics can be described with a set of nonlinear DAEs. Using an implicit form:

$$\mathbf{0}_{(\nu+\mu)\times 1} = \boldsymbol{\phi}(\boldsymbol{x}', \boldsymbol{x}, \boldsymbol{y})\,. \tag{1}$$

In (1), $\boldsymbol{x} = \boldsymbol{x}(t) : [0, \infty) \to \mathbb{R}^{\nu}$ and $\boldsymbol{y} = \boldsymbol{y}(t) : [0, \infty) \to \mathbb{R}^{\mu}$ are the state and algebraic variables, respectively, of the system; $\boldsymbol{\phi} : \mathbb{R}^{\nu+\mu} \to \mathbb{R}^{\nu+\mu}$ are nonlinear functions; $\mathbf{0}_{(\nu+\mu)\times 1}$ denotes the zero matrix

of dimensions $(\nu + \mu) \times 1$. Differential and algebraic equations are commonly expressed as two distinct sets, i.e., using the Hessenberg form [8]:

$$\begin{aligned} \boldsymbol{x}' &= \boldsymbol{f}(\boldsymbol{x}, \boldsymbol{y}) \,, \\ \boldsymbol{0}_{\mu \times 1} &= \boldsymbol{g}(\boldsymbol{x}, \boldsymbol{y}) \,, \end{aligned} \tag{2}$$

where $\boldsymbol{f} : \mathbb{R}^{\nu+\mu} \to \mathbb{R}^{\nu}$ and $\boldsymbol{g} : \mathbb{R}^{\nu+\mu} \to \mathbb{R}^{\mu}$ define, respectively, the system's differential and algebraic equations.

Approximating the solution of (2) for a set of known initial conditions requires performing a time-domain simulation through the application of a proper discrete TDI method. Implicit ODE methods are commonly preferred from explicit ones due to their ability to handle system stiffness, as well as due to their numerical stability properties. We recall here that the stability properties of implicit ODE methods are not guaranteed to hold when applied to DAEs, but rather transfer better to DAEs with a small differentiation index [23–25]. We note that DAEs (2) are index-1[1] if $(\boldsymbol{x}, \boldsymbol{y}) := [\boldsymbol{x}^\intercal, \boldsymbol{y}^\intercal]^\intercal$ (where $^\intercal$ is the matrix transpose) is differentiable and $\boldsymbol{g}_y = \partial \boldsymbol{g} / \partial \boldsymbol{y}$ is not singular at every t along the solution flow.

In this paper, we employ the well-known Theta method for the TDI of (2). In this case, discretization is implemented through the following linear fractional transformation:

$$z = \frac{1 + h\theta s}{1 - h(1-\theta)s} \Leftrightarrow s = \frac{1}{h} \frac{z - 1}{(1-\theta)z + \theta} \,, \tag{3}$$

where s and z are the complex variables of the s-domain and z-domain, respectively; h is the integration time step size; and θ defines the method's damping. Applied to (2), the Theta method reads as follows:

$$\begin{aligned} \boldsymbol{x}_{n+1} &= \boldsymbol{x}_n + h[\theta \boldsymbol{f}(\boldsymbol{x}_n, \boldsymbol{y}_n) + (1-\theta)\boldsymbol{f}(\boldsymbol{x}_{n+1}, \boldsymbol{y}_{n+1})] \,, \\ \boldsymbol{0}_{\mu \times 1} &= \boldsymbol{g}(\boldsymbol{x}_{n+1}, \boldsymbol{y}_{n+1}) \,. \end{aligned} \tag{4}$$

For the sake of completeness, the derivation of (4) from (2) and (3) is provided in Section Appendix A of the Appendix. Note that (4) in fact describes a family of TDI methods. Methods commonly used in power system simulation software arise from (4) as special cases. For example, $\theta = 0.5$ gives the trapezoidal method (TM), while $\theta = 0$ gives the backward Euler method (BEM).

Given the value of $(\boldsymbol{x}_n, \boldsymbol{y}_n)$ at some time in the simulation, the method computes at each step the new value $(\boldsymbol{x}_{n+1}, \boldsymbol{y}_{n+1})$, which is an approximation of the exact solution of (2), i.e.:

$$\begin{aligned} \boldsymbol{x}_{n+1-\ell} &\approx \boldsymbol{x}(t + (1-\ell)h) \,, \\ \boldsymbol{y}_{n+1-\ell} &\approx \boldsymbol{y}(t + (1-\ell)h) \,, \end{aligned} \tag{5}$$

[1] The differentiation index q of a DAE set in the form of (2) is defined as the highest order of time derivative d^q/dt^q required to to eliminate the algebraic constraints.

where $\boldsymbol{x}_{n+1-\ell} : \mathbb{N} \to \mathbb{R}^{\nu}$, $\boldsymbol{y}_{n+1-\ell} : \mathbb{N} \to \mathbb{R}^{\mu}$ are the discretized state and algebraic variables, respectively, at time $t+(1-l)h$, with $l \in \mathbb{N}$ and $n = t/h$. The solution $(\boldsymbol{x}_{n+1}, \boldsymbol{y}_{n+1})$ at each step is typically obtained through Newton iterations.

2.2 DDAE Power System Model

If time delays are present in the system, the set of DAEs (2) changes into a set of DDAEs. Using a Hessenberg form, we have:

$$\begin{aligned} \boldsymbol{x}' &= \boldsymbol{f}(\boldsymbol{x}, \boldsymbol{y}, \boldsymbol{x}_d, \boldsymbol{y}_d)\,, \\ \boldsymbol{0}_{\mu\times 1} &= \boldsymbol{g}(\boldsymbol{x}, \boldsymbol{y}, \boldsymbol{x}_d, \boldsymbol{y}_d)\,, \end{aligned} \tag{6}$$

with:

$$\begin{aligned} \boldsymbol{x}_d &= \{\boldsymbol{x}(t-\tau_1), \boldsymbol{x}(t-\tau_2), \ldots, \boldsymbol{x}(t-\tau_m)\}\,, \\ \boldsymbol{y}_d &= \{\boldsymbol{y}(t-\tau_1), \boldsymbol{y}(t-\tau_2), \ldots, \boldsymbol{y}(t-\tau_m)\}\,, \end{aligned} \tag{7}$$

where $\tau_i > 0$, $i = 1, 2, \ldots, m$, is the i-th time delay of the system and m is the total number of delays. Note that (6) is not index-1 [26]. Under the assumption that $\boldsymbol{g}_y = \partial \boldsymbol{g}/\partial \boldsymbol{y}$ is not singular at every t, an index-1 DDAE model can be constructed if it is additionally assumed that retarded algebraic variables do not appear in the algebraic equations. In this paper we refrain from this assumption and work with the more general system (6). We also note that (6) assumes a constant delay model, which suffices to study the impact on numerical stability and comes without loss of generality. A detailed discussion on modeling and analysis of systems with time-varying delays that include noise, periodicity and data packet dropouts, can be found in [4, 7].

We proceed to provide the formulation of the Theta method for the solution of system (6). Applying the Laplace transform to (6) and omitting for simplicity the initial conditions:

$$\begin{aligned} s\mathcal{L}\{\boldsymbol{x}\} &= \mathcal{L}\{\boldsymbol{f}(\boldsymbol{x}, \boldsymbol{y}, \boldsymbol{x}_d, \boldsymbol{y}_d)\}\,, \\ \boldsymbol{0}_{\mu\times 1} &= \mathcal{L}\{\boldsymbol{g}(\boldsymbol{x}, \boldsymbol{y}, \boldsymbol{x}_d, \boldsymbol{y}_d)\}\,. \end{aligned} \tag{8}$$

We first consider the simplest case where a single delay τ is present in the system, i.e.:

$$\begin{aligned} \boldsymbol{x}_d &= \boldsymbol{x}(t-\tau), \\ \boldsymbol{y}_d &= \boldsymbol{y}(t-\tau). \end{aligned} \tag{9}$$

We then apply the linear fractional transformation (3) to (8). In the discrete-time system that arises, delays that are not multiples of the time step, that is, $kh < \tau < (k+1)h,\ k \in \mathbb{N}$, are handled with linear interpolation between kh and $(k+1)h$. For example, for a given retarded variable $v(t-\tau)$, we use the

approximation:

$$\begin{aligned} v(t-\tau) &= c\, v(t-kh) + (1-c)\, v(t-(k+1)h) \; + \mathcal{O}(h^2) \\ &\approx c\, v_{n-k} + (1-c)\, v_{n-(k+1)}\,, \end{aligned} \tag{10}$$

where $\mathcal{O}(h^2)$ denotes the linear interpolation error and the coefficient c is given by:

$$c = \frac{(k+1)h - \tau}{h}\,.$$

From (5), (3), we arrive to the following expression:

$$\begin{aligned} (z-1)\mathcal{Z}\{\boldsymbol{x}_n\} &= h(\theta + (1-\theta)z)\mathcal{Z}\{\boldsymbol{f}(\boldsymbol{x}_n, \boldsymbol{y}_n, \boldsymbol{\mathcal{V}}_k^{k+1})\}\,, \\ \mathbf{0}_{\mu\times 1} &= \mathcal{Z}\{\boldsymbol{g}(\boldsymbol{x}_{n+1}, \boldsymbol{y}_{n+1}, \boldsymbol{\mathcal{V}}_k^{k+1})\}\,, \end{aligned} \tag{11}$$

where $\mathcal{Z}\{\cdot\}$ denotes the Z-transform and $\boldsymbol{\mathcal{V}}_k^{k+1}$ denoting the following set of variables:

$$\boldsymbol{\mathcal{V}}_k^{k+1} = \{\boldsymbol{x}_{n-k}, \boldsymbol{y}_{n-k}, \boldsymbol{x}_{n-(k+1)}, \boldsymbol{y}_{n-(k+1)}\}\,,\; k \in \mathbb{N}.$$

Applying the inverse Z-transform to (11), we obtain:

$$\begin{aligned} \boldsymbol{x}_{n+1} &= \boldsymbol{x}_n + h\theta \boldsymbol{f}(\boldsymbol{x}_n, \boldsymbol{y}_n, \boldsymbol{\mathcal{V}}_k^{k+1}) \\ &\qquad + h(1-\theta)\boldsymbol{f}(\boldsymbol{x}_{n+1}, \boldsymbol{y}_{n+1}, \boldsymbol{\mathcal{V}}_{k-1}^{k})\,, \\ \mathbf{0}_{\mu\times 1} &= \boldsymbol{g}(\boldsymbol{x}_{n+1}, \boldsymbol{y}_{n+1}, \boldsymbol{\mathcal{V}}_{k-1}^{k})\,. \end{aligned} \tag{12}$$

Equation (12) is the discrete equivalent of (6), approximated by the Theta method, when only a single delay is present in the system. This equation can be then conveniently generalized for the multiple-delay case. In particular, for a total number of m delays τ_i, with $k_i h \leq \tau_i < (k_i+1)h$, $i = \{1, 2, \ldots, m\}$ and $k_i \in \mathbb{N}$, application of the linear fractional transformation (3) to (8) yields:

$$\begin{aligned} \boldsymbol{x}_{n+1} &= \boldsymbol{x}_n + h\theta \boldsymbol{f}(\boldsymbol{x}_n, \boldsymbol{y}_n, \boldsymbol{\mathcal{V}}_{k_1}^{k_1+1}, \ldots, \boldsymbol{\mathcal{V}}_{k_m}^{k_m+1}) \\ &\qquad + h(1-\theta)\boldsymbol{f}(\boldsymbol{x}_{n+1}, \boldsymbol{y}_{n+1}, \boldsymbol{\mathcal{V}}_{k_1-1}^{k_1}, \ldots, \boldsymbol{\mathcal{V}}_{k_{m-1}}^{k_m})\,, \\ \mathbf{0}_{\mu\times 1} &= \boldsymbol{g}(\boldsymbol{x}_{n+1}, \boldsymbol{y}_{n+1}, \boldsymbol{\mathcal{V}}_{k_1-1}^{k_1}, \ldots, \boldsymbol{\mathcal{V}}_{k_{m-1}}^{k_m})\,. \end{aligned} \tag{13}$$

The main concept discussed in this paper is that, being implicit notwithstanding, (13) can perform poorly and even become numerically unstable when applied to a power system model with inclusion of multiple delayed variables. The above behavior is attributed to the fact that the properties of the standard implicit TDI methods are altered in the present of retarded variables. The extent of the distortion depends on the number and the strength of the coefficients of those variables in the DDAEs. This is illustrated theoretically through numerical stability analysis, in Section 3, as well as through

numerical simulations in the case study of Section 4.

3 Numerical Stability Analysis

In this section, we first illustrate through numerical stability analysis of a scalar test equation that standard implicit ODE methods can become unstable when applied to a time-delayed system. We then proceed to describe a matrix pencil approach to study the conditions under which such numerical instabilities can arise in the simulation of realistic power system models.

3.1 Analytical Study of Test Delay Differential Equation

The standard approach to study the stability properties of a numerical TDI method for ODEs is to evaluate its response when applied to the linear test differential equation:

$$x'(t) = ax(t)\,, \quad a \in \mathbb{C}\,. \tag{14}$$

Applying the Theta method to (14) we have:

$$x_{n+1} = \frac{1 + h\theta a}{1 - h(1-\theta)a} x_n\,, \tag{15}$$

where

$$\mathcal{R}(ah) = \frac{1 + h\theta a}{1 - h(1-\theta)a}\,, \tag{16}$$

is the method's *growth function*. The stability region of the method is defined by the set $\{a \in \mathbb{C} : |\mathcal{R}(ah)| < 1\}$. For example, $\theta = 0.5$ gives the TM, for which:

$$\mathcal{R}(ah) = \frac{1 + 0.5ha}{1 - 0.5ha}\,. \tag{17}$$

The stability region in this case is $\mathrm{Re}\{ah\} < 0 :\ ah \in \mathbb{C}$, i.e., the open left half of the s-plane (symmetrical A-stability).

Let's consider that a time delay $\tau = h$ is introduced to (14). Then, the latter changes into the following test delay differential equation:

$$x'(t) = ax(t) + bx(t-h)\,, \tag{18}$$

Application of the Theta method to (18) gives:

$$x_{n+1} = \frac{1 + ah\theta + bh(1-\theta)}{1 - ah(1-\theta)} x_n + \frac{bh\theta}{1 - ah(1-\theta)} x_{n-1}\,. \tag{19}$$

By setting $\boldsymbol{\psi}_n = [x_n, x_{n-1}]^\intercal$, (19) can be expressed in the form:

$$\boldsymbol{\psi}_{n+1} = \boldsymbol{\mathcal{R}}\, \boldsymbol{\psi}_n \ , \tag{20}$$

where:

$$\boldsymbol{\mathcal{R}} = \begin{bmatrix} \dfrac{1 + ah\theta + bh(1-\theta)}{1 - ah(1-\theta)} & \dfrac{bh\theta}{1 - ah(1-\theta)} \\ 1 & 0 \end{bmatrix} . \tag{21}$$

The stability region of the Theta method when applied to (18) can thus be determined through the eigenvalues of matrix $\boldsymbol{\mathcal{R}}$. In particular, the method is stable in the region for which $\rho(\boldsymbol{\mathcal{R}}) < 1$, where $\rho(\cdot)$ denotes the spectral radius of a matrix.

As already discussed in Section 2, two important elements of the family of integration schemes that the Theta method covers are obtained for $\theta = 0$ (BEM) and $\theta = 0.5$ (TM). Figures 1 and 2 illustrate the numerical stability regions of these methods when applied to (18), considering different weights a and b for the delay-free and delayed parts of the equation, respectively. In particular, Figs. 1a and 2a show the stability regions for $b = 0$, in which case (18) is reduced to the test ODE (14). As it is well-known, the stability region of the BEM for ODEs lies outside the unit circle centered at $(1, 0)$ of the complex plane, and the method is L-stable. Moreover, the stability region of the TM for ODEs is the open left half of the complex plane, and the method is symmetrically A-stable.

The above important numerical stability properties do not extend to time-delayed systems. The extreme theoretical scenario is $a = 0$, in which case the evolution of the present state in (18) is influenced solely by the past value $x(t-h)$. In this scenario, both BEM and TM are *unstable*. As a matter of fact, the stability region of the BEM in this case is identical to that of the explicit Euler method for ODEs. Then, the plots in Figs. 1b-1f basically illustrate that the BEM is numerically stable only if $a \geq b$. Most importantly, Figs. 2b-2f indicate that, for $b \neq 0$, there exists a time step size $h > 0$ above which the TM is destabilized. In fact, the stability region of the method shrinks as the ratio b/a is increased, i.e., the risk for numerical instability becomes higher, as the influence of the past state on $x'(t)$ gets stronger.

Extrapolating these observations to a time-delayed system, one can expect that the number of delayed variables and the magnitudes of their coefficients have a crucial impact on the stability region of the Theta method applied. Then, in power system models with a large number of non-negligible delayed variables, there are expected to be cases for which e.g., the TM significantly deforms the system's dynamic modes even for reasonably small time step sizes, potentially making stable trajectories appear as unstable. Needless to say, the specific conditions under which such numerical issues arise will be system dependent. The question is then how to study the numerical deformation introduced by the integration method to the dynamics of a given power system model that includes multiple delayed variables. This is discussed in detail in the next paragraph.

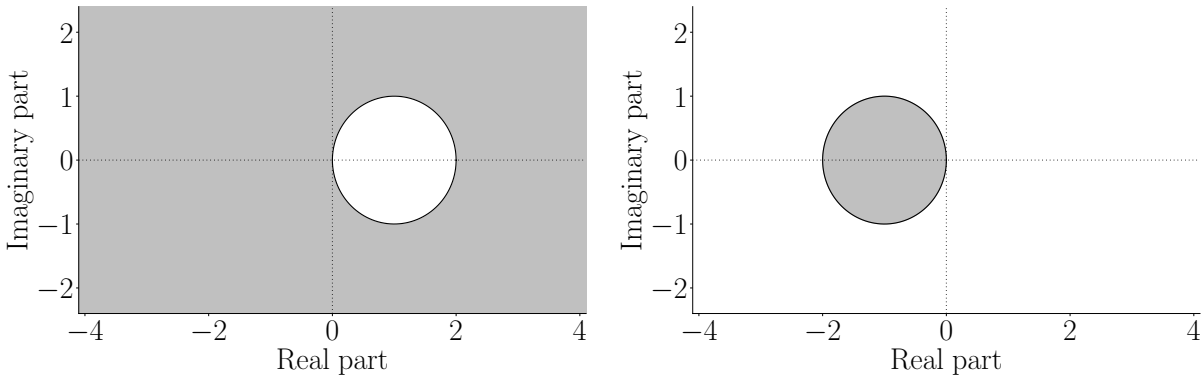

(a) $a \in \mathbb{C},\ b = 0 :\ x' = a\, x(t)$

(b) $a = 0,\ b \in \mathbb{C} :\ x' = b\, x(t-h)$

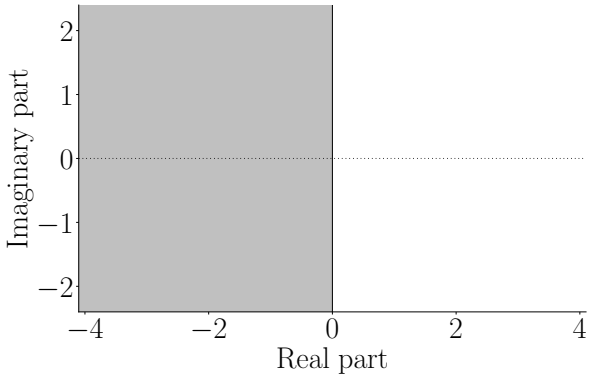

(c) $a \in \mathbb{C},\ b = a :\ x' = a\, x(t) + a\, x(t-h)$

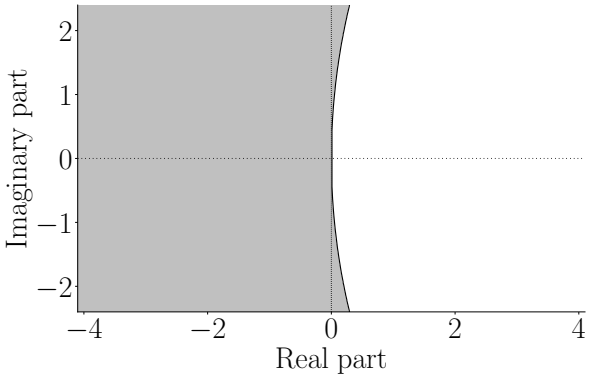

(d) $b \in \mathbb{C},\ a = 1.1\, b :\ x' = 1.1\, b\, x(t) + b\, x(t-h)$

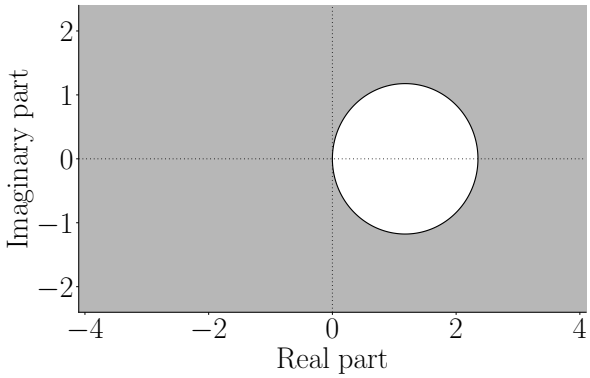

(e) $a \in \mathbb{C},\ b = 0.15\, a :\ x' = a\, x(t) + 0.15\, a\, x(t-h)$

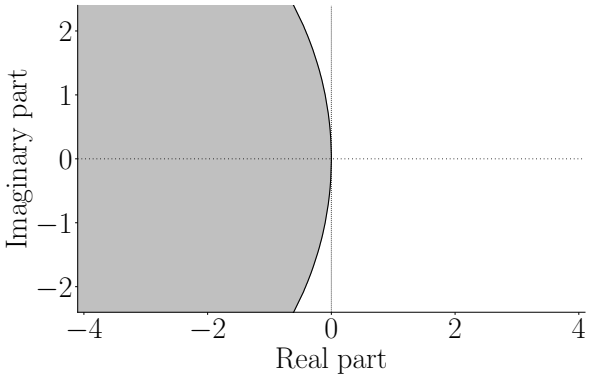

(f) $b \in \mathbb{C},\ a = 0.85\, b :\ x' = 0.85 b\, x(t) + b\, x(t-h)$

Figure 1: Numerical stability region (gray area) for test equation (18), $\theta = 0$ (BEM).

3.2 Systems with Multiple Time-Delayed Variables

For a scalar test equation, such as (18) discussed above, one can characterize analytically the properties of Theta method by identifying its numerical stability region (e.g., see Figs. 1, 2). However, real-world power system models are too large in size and too complex to permit calculation of numerical TDI stability regions. In this section, we address this limitation of standard numerical stability analysis techniques, by describing a small-signal stability analysis (SSSA)-based approach to capture the impact of delays on the behavior of the Theta method when applied to a dynamic power system model.

Consider the DDAE power system model (6) and assume that a stationary solution $(\boldsymbol{x}_o, \boldsymbol{y}_o)$ is known.

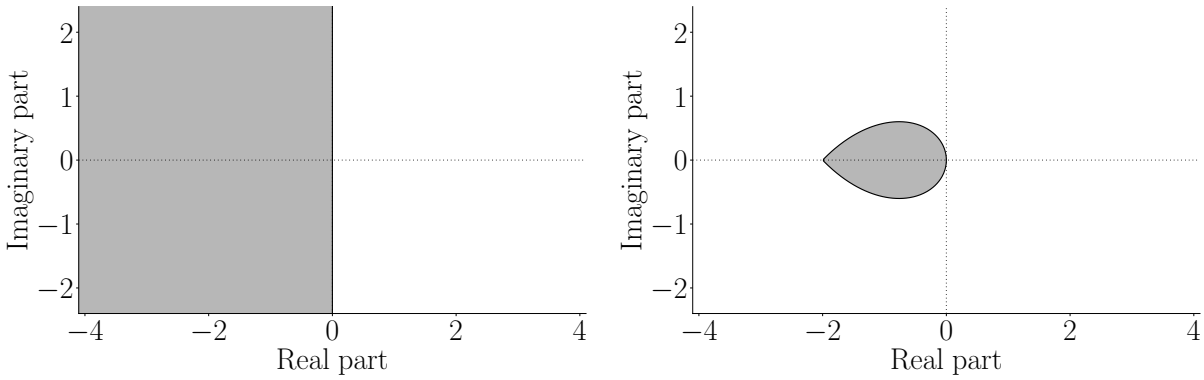

(a) $a \in \mathbb{C},\ b = 0 :\ x' = a\, x(t)$

(b) $a = 0,\ b \in \mathbb{C} :\ x' = b\, x(t-h)$

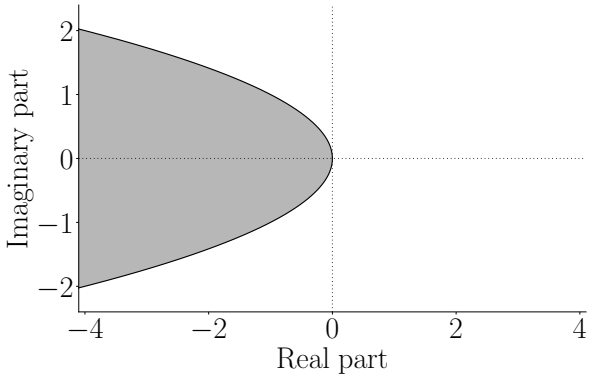

(c) $a \in \mathbb{C},\ b = a :\ x' = a\, x(t) + a\, x(t-h)$

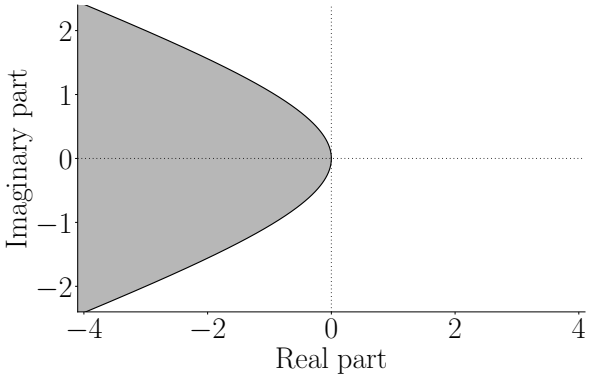

(d) $b \in \mathbb{C},\ a = 1.1\, b :\ x' = 1.1\, b\, x(t) + b\, x(t-h)$

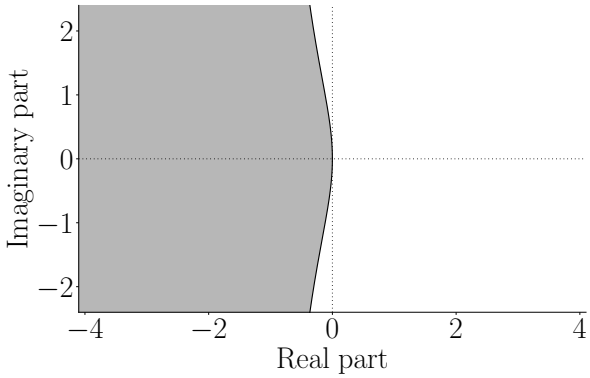

(e) $a \in \mathbb{C},\ b = 0.15\, a :\ x' = a\, x(t) + 0.15\, a\, x(t-h)$

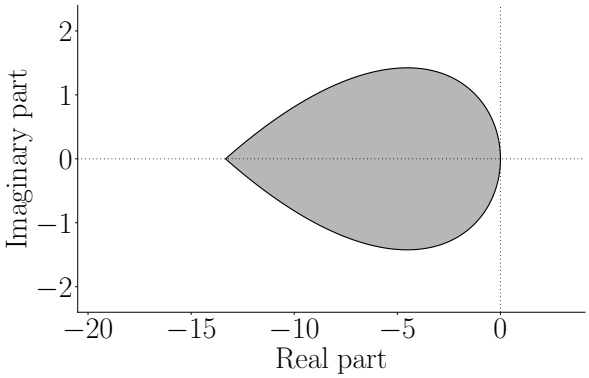

(f) $b \in \mathbb{C},\ a = 0.85\, b :\ x' = 0.85 b\, x(t) + b\, x(t-h)$

Figure 2: Numerical stability region (gray area) for test equation (18), $\theta = 0.5$ (TM).

We denote $\tilde{\boldsymbol{x}} = \boldsymbol{x} - \boldsymbol{x}_o$ and $\tilde{\boldsymbol{y}} = \boldsymbol{y} - \boldsymbol{y}_o$. Then, differentiating (6) at the stationary point yields:

$$\begin{aligned} \tilde{\boldsymbol{x}}' &= \boldsymbol{f}_x \tilde{\boldsymbol{x}} + \boldsymbol{f}_y \tilde{\boldsymbol{y}} + \sum_{i=1}^{m} [\boldsymbol{f}_{x,i} \tilde{\boldsymbol{x}}(t-\tau_i) + \boldsymbol{f}_{y,i} \tilde{\boldsymbol{y}}(t-\tau_i)]\,, \\ \boldsymbol{0}_{\mu\times 1} &= \boldsymbol{g}_x \tilde{\boldsymbol{x}} + \boldsymbol{g}_y \tilde{\boldsymbol{y}} + \sum_{i=1}^{m} [\boldsymbol{g}_{x,i} \tilde{\boldsymbol{x}}(t-\tau_i) + \boldsymbol{g}_{y,i} \tilde{\boldsymbol{y}}(t-\tau_i)]\,, \end{aligned} \tag{22}$$

where $(\boldsymbol{f}_x,\ \boldsymbol{f}_y,\ \boldsymbol{g}_x,\ \boldsymbol{g}_y)$ and $(\boldsymbol{f}_{x,i},\ \boldsymbol{f}_{y,i},\ \boldsymbol{g}_{x,i},\ \boldsymbol{g}_{y,i})$ denote the delay-free and the delayed Jacobians for

$\tau = \tau_i$ respectively. By setting $\tilde{\mathbf{x}} = (\tilde{\boldsymbol{x}}, \tilde{\boldsymbol{y}})$, (22) becomes equivalently:

$$\mathbf{E}\tilde{\mathbf{x}}' = \mathbf{A}_0\tilde{\mathbf{x}} + \sum_{i=1}^{m} \mathbf{A}_i\tilde{\mathbf{x}}(t-\tau_i)\,, \tag{23}$$

where:

$$\mathbf{E} = \begin{bmatrix} \boldsymbol{I}_\nu & \mathbf{0}_{\nu\times\mu} \\ \mathbf{0}_{\mu\times\nu} & \mathbf{0}_{\mu\times\mu} \end{bmatrix},\ \mathbf{A}_0 = \begin{bmatrix} \boldsymbol{f}_x & \boldsymbol{f}_y \\ \boldsymbol{g}_x & \boldsymbol{g}_y \end{bmatrix},\ \mathbf{A}_i = \begin{bmatrix} \boldsymbol{f}_{x,i} & \boldsymbol{f}_{y,i} \\ \boldsymbol{g}_{x,i} & \boldsymbol{g}_{y,i} \end{bmatrix},$$

where $\boldsymbol{I}_\nu$ is the identity matrix of size ν. The eigenvalues of (23) are the roots of the determinant of the system's matrix pencil, which is defined as follows [26]:

$$s\mathbf{E} - \mathbf{A}_0 - \sum_{i=1}^{m} \mathbf{A}_i e^{-s\tau_i} \tag{24}$$

We note that the time delays present in (22) give rise to exponential terms in (24). This suggests the existence of infinitely many characteristic roots [26], the calculation of which is prohibitive. There are various approaches in the existing literature to overcome this issue. The experience of the authors is that arguably the most effective one is to compute an approximately equivalent linear pencil through the application of spectral discretization. The procedure is described in detail in [26], and includes two steps: first, the linearized DDAE system is transformed into an equivalent system of partial differential equations (PDEs); then, the PDE system is reduced to a linear eigenvalue problem of finite dimensions, through Chebyshev polynomials. The order N of the polynomials improves the accuracy of the eigenvalues' computation. The Chebyshev discretization order in the case study of Section 4 has been specified as $N = 10$, which, based on our previous experience on finding the spectra of DDAEs is sufficient to ensure highly accurate results. Boundary conditions are inherently defined by the DDAE formulation. A detailed description of the spectral discretization technique followed in this paper can be found in [27].

Applying the Theta method to (22):

$$\begin{aligned} \tilde{\boldsymbol{x}}_{n+1} = \tilde{\boldsymbol{x}}_n &+ h(1-\theta)(\hat{\boldsymbol{f}}_x\tilde{\boldsymbol{x}}_{n+1} + \hat{\boldsymbol{f}}_y\tilde{\boldsymbol{y}}_{n+1}) \\ &+ h\theta(\hat{\boldsymbol{f}}_x\tilde{\boldsymbol{x}}_n + \hat{\boldsymbol{f}}_y\tilde{\boldsymbol{y}}_n) \\ &+ h(1-\theta)\sum_{k=1}^{r}(\hat{\boldsymbol{f}}_{x,k}\tilde{\boldsymbol{x}}_{n+1-k} + \hat{\boldsymbol{f}}_{y,k}\tilde{\boldsymbol{y}}_{n+1-k}) \\ &+ h\theta\sum_{k=1}^{r}(\hat{\boldsymbol{f}}_{x,k}\tilde{\boldsymbol{x}}_{n-k} + \hat{\boldsymbol{f}}_{y,k}\tilde{\boldsymbol{y}}_{n-k})\,, \end{aligned}$$

$$\mathbf{0}_{\mu\times 1} = [\hat{\boldsymbol{g}}_x\tilde{\boldsymbol{x}}_{n+1} + \hat{\boldsymbol{g}}_y\tilde{\boldsymbol{y}}_{n+1}] + \sum_{k=1}^{r}(\hat{\boldsymbol{g}}_{x,k}\tilde{\boldsymbol{x}}_{n+1-k} + \hat{\boldsymbol{g}}_{y,k}\tilde{\boldsymbol{y}}_{n+1-k})\,,$$

Delays in the above equations appear as multiples of the time step as the delay-free ($\hat{\boldsymbol{f}}_x$, $\hat{\boldsymbol{f}}_y$, $\hat{\boldsymbol{g}}_x$, $\hat{\boldsymbol{g}}_y$) and delayed ($\hat{\boldsymbol{f}}_{x,k}$, $\hat{\boldsymbol{f}}_{y,k}$, $\hat{\boldsymbol{g}}_{x,k}$, $\hat{\boldsymbol{g}}_{y,k}$) Jacobian matrices are formulated to account for delay interpolation according to (10). Moreover, the upper limit of summation r is such that $r \in \mathbb{N}^+$: $(r-1)h < \tau_{\max} \leq rh$, where $\tau_{\max}$ is the delay with the largest magnitude. Equivalently:

$$\mathbf{M}\mathbf{x}_{n+1} = \mathbf{A}\mathbf{x}_n + \sum_{k=1}^{r}\left(\mathbf{B}_{k-1}\mathbf{x}_{n-(k-1)} + \mathbf{C}_k\mathbf{x}_{n-k}\right)\,, \tag{25}$$

where $\mathbf{x}_n = (\tilde{\boldsymbol{x}}_n, \tilde{\boldsymbol{y}}_n)$ and:

$$\mathbf{M} = \begin{bmatrix} \boldsymbol{I}_\nu - h(1-\theta)\hat{\boldsymbol{f}}_x & -h(1-\theta)\hat{\boldsymbol{f}}_y \\ -\hat{\boldsymbol{g}}_x & -\hat{\boldsymbol{g}}_y \end{bmatrix},$$

$$\mathbf{A} = \begin{bmatrix} \boldsymbol{I}_\nu + h\theta\hat{\boldsymbol{f}}_x & h\theta\hat{\boldsymbol{f}}_y \\ \mathbf{0}_{\mu\times\nu} & \mathbf{0}_{\mu\times\mu} \end{bmatrix},$$

$$\mathbf{B}_{k-1} = \begin{bmatrix} h(1-\theta)\hat{\boldsymbol{f}}_{x,k} & h(1-\theta)\hat{\boldsymbol{f}}_{y,k} \\ \hat{\boldsymbol{g}}_{x,k} & \hat{\boldsymbol{g}}_{y,k} \end{bmatrix},$$

$$\mathbf{C}_k = \begin{bmatrix} h\theta\hat{\boldsymbol{f}}_{x,k} & h\theta\hat{\boldsymbol{f}}_{y,k} \\ \mathbf{0}_{\mu\times\nu} & \mathbf{0}_{\mu\times\mu} \end{bmatrix},$$

which can be rewritten in the form:

$$\mathbf{F}\,\boldsymbol{\psi}_{n+1} = \mathbf{G}\,\boldsymbol{\psi}_n\,. \tag{26}$$

The proof of (26) is provided in Section Appendix B of the Appendix.

Equation (26) is a discrete-time approximation of (23), where $\mathbf{F}$ and $\mathbf{G}$ vary for different values of θ but are always matrix functions of $\mathbf{A}$ and h. The matrix pencil of (26) is:

$$\hat{z}\mathbf{F} - \mathbf{G}\,. \tag{27}$$

We quantify the numerical deformation introduced by the Theta method to the power system dynamics by comparing the eigenvalues of (27) with those of (24). In this regard, note that the eigenvalues of (27) lie in the z-domain whereas those of (22) in the s-domain. Thus, to make the results comparable, we

transform the roots of (27) to the s-domain, through the logarithmic transformation:

$$\hat{s} = \frac{1}{h} \ln \hat{z}\,, \tag{28}$$

where $\hat{s}$ and $\hat{z}$ represent the numerically deformed eigenvalues in the s-domain and z-domain respectively. Numerical instability is identified when a deformed eigenvalue $\hat{s}$ lies in the positive half of the complex plane, while the real parts of all finite eigenvalues of (22) remain negative. A flowchart of the matrix pencil approach used for estimating the numerical deformation introduced by the Theta method is shown in Fig. 3.

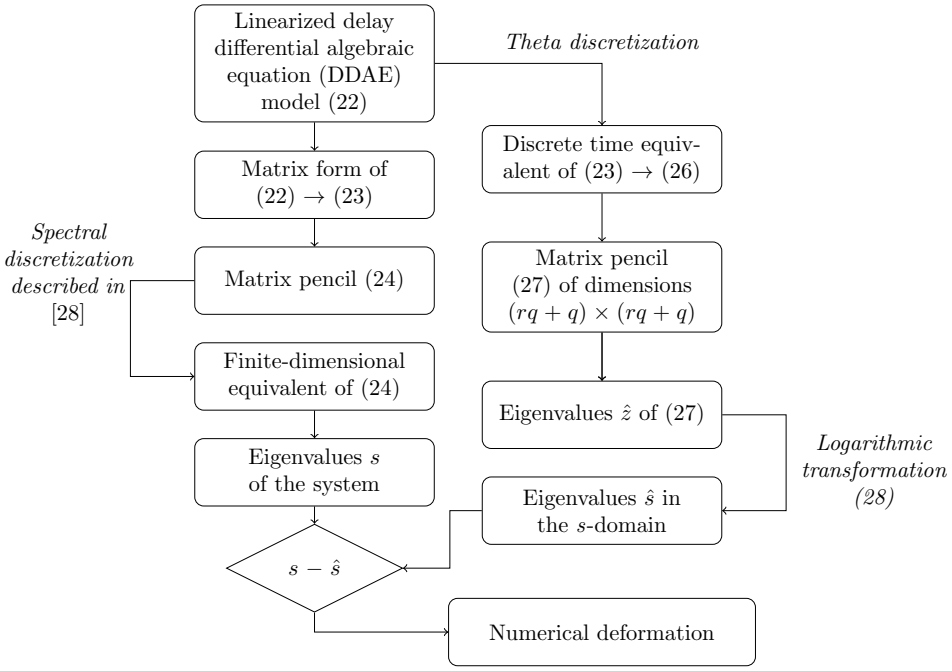

Figure 3: Flowchart of matrix pencil-based analysis.

The approach above is based on SSSA and hence the results are in principle valid only in a neighborhood around equilibria. Nevertheless, when numerical instability is predicted, it is guaranteed to occur, as instability observed for small disturbances inherently implies instability under larger disturbances as well. Moreover, the structure and stiffness of power systems as well as the properties of TDI methods are features that tend to be robust with respect to the operating condition, and thus the results provide a tentative yet accurate estimate of numerical deformation also for varying operating conditions. Similar considerations can be found in the literature, e.g., see [20, 28, 29].

4 Case Study

This section first presents simulation results based on the IEEE 39-bus system, detailed data of which can be found in [30]. Its dynamic models are thoroughly presented in [31]. The original system consists

of 10 synchronous machines (SMs), modeled by fourth order, two-axis models, 34 transmission lines, 12 transformers and 19 loads. Each machine is equipped with an automatic voltage regulator (AVR), a turbine governor (TG) and a power system stabilizer (PSS). Moreover, SMs are assumed to provide secondary frequency regulation through an automatic generation control (AGC) system modeled as an integral controller with gain $\mathrm{k}_0 = 1$. The resulting model has in total 393 variables (131 states and 262 algebraic variables). Then, aiming to address the limitations and the computational efficiency of the matrix pencil approach described in Section 3, we present simulation results based on a large-scale model, namely the All-Island Irish Transmission System (AIITS)

Simulation results in this section are produced using the the Python-based power system analysis software tool Dome [32]. The version of the software employed in this paper relies on LAPACK 3.10.0 for QR factorization and the KLU 5.10.1 for LU factorization. The error tolerance during TDI simulations is 10^{-5} and the maximum number of Newton iterations is set equal to 20.

4.1 Delay-Free 39-Bus System

We first consider the system without delays. The stiffness of the examined system is measured through the ratio $\mathcal{S} = |s^{\max}|/|s^{\min}|$ between the largest and smallest eigenvalue magnitudes $|s^{\max}|$ and $|s^{\min}|$ of the corresponding linearized model. In our case, $\mathcal{S} = 5300.53$. The examined system is small-signal stable and the two rightmost pairs of eigenvalues are $s_{1,2} = -0.694176 \pm j0.808851$ with damping ratio $\zeta_{1,2} = 65.1\%$ and $s_{3,4} = -0.013359 \pm j0.050441$ with damping ratio $\zeta_{3,4} = 25.6\%$.

We illustrate how the Theta method deforms numerically the dynamic modes of the system as the integration time step varies in the range $h \in [0.001, 0.5]$ s. In particular, Fig. 4a shows the numerical deformation of the most critical system modes (represented by the rightmost eigenvalues) for $\theta = 0.5$ (TM). To track the positions of the numerically deformed eigenvalues $\hat{s}$ and ensure they are ordered in a consistent way, we check both the Euclidean distances of eigenvalues as well as the variations of the associated modal participation factors. Figures 4b–4c show a close-up of $s_1 = -0.694176 + j0.808851$ and $s_3 = -0.013359 + j0.050441$, with the corresponding numerically deformed eigenvalues being denoted with $\hat{s}_1$ and $\hat{s}_3$, respectively. The plots indicate that the TM is very accurate to approximate the system dynamics for small time steps, whereas for very large steps it introduces spurious underdamping, yet without compromising numerical stability, as the numerically deformed system retains the stability of the real one regardless of the magnitude of h.

Decreasing the parameter θ to values smaller than 0.5 leads to numerical methods with higher damping. For example, setting $\theta = 0$ corresponds to the BEM, which strongly overdamps all system modes. However, not all modes are ensured to be overdamped for $0 < \theta < 0.5$. This is especially true for values close to 0.5, which is also a common choice in commercial software implementations [11]. For example, setting $\theta = 0.49$ introduces a dichotomy in the response of the Theta method, where most modes get nu-

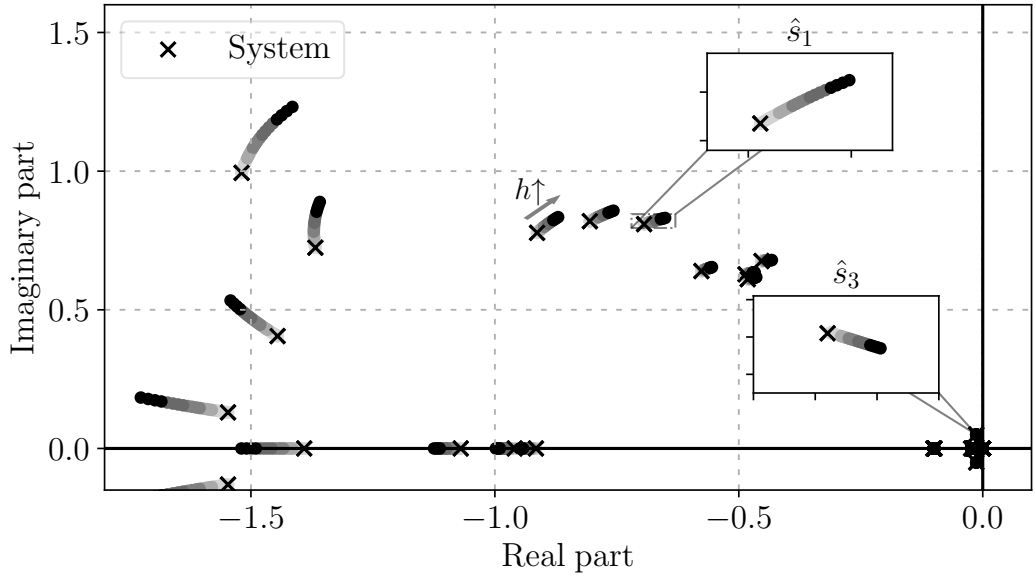

(a) Rightmost eigenvalues.

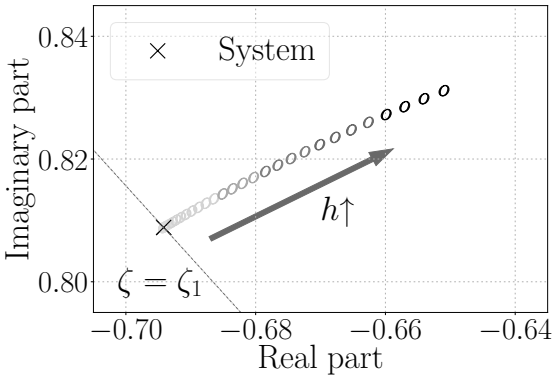

(b) Close-up for eigenvalue $\hat{s}_1$.

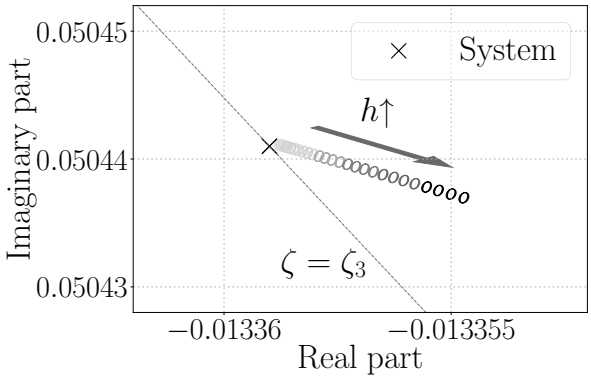

(c) Close-up for eigenvalue $\hat{s}_3$.

Figure 4: Delay-free system: Eigenvalue numerical deformation under the effect of the TM ($\theta = 0.5$).

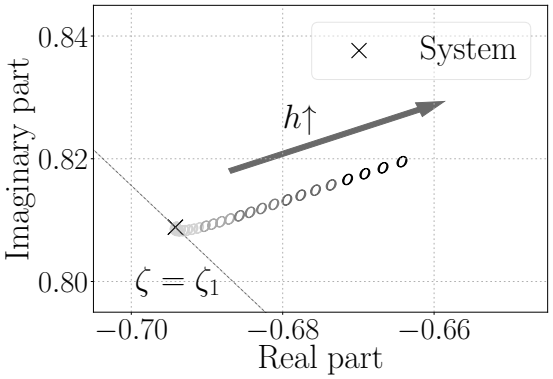

(a) Close-up for eigenvalue $\hat{s}_1$.

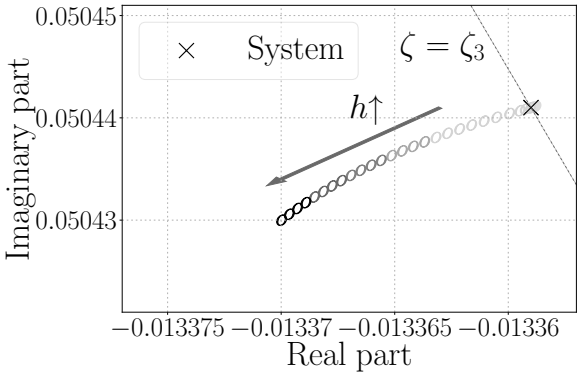

(b) Close-up for eigenvalue $\hat{s}_3$.

Figure 5: Delay-free system: Eigenvalue numerical deformation under the effect of the Theta method, for $\theta = 0.49$.

merically underdamped as h increases (like s_1 in Fig. 5a) yet there also exist modes that appear slightly overdamped (e.g., s_3 in Fig. 5b). To further confirm the validity of these results, we carry out a TDI of

the nonlinear system model considering a three-phase fault at bus 6 occurring at $t = 1.0$ s and cleared after 80 ms by opening the line that connects buses 5 and 6. Figure 6 shows the rotor speed of SM 3, which is the variable associated to $s_{3,4}$ with the largest participation factor. The figure indeed indicates that the damping of the obtained oscillation is higher for larger time steps. Based on Fig. 6, we estimate the numerical error accumulation over time using a reference trajectory obtained with $h = 0.0001$ s and for a duration of 15 s. For $h = 0.001$ s, the maximum and average errors are $7.4 \cdot 10^{-6}$ and $1.2 \cdot 10^{-7}$, respectively, while for $h = 0.07$ s, they are $3.7 \cdot 10^{-4}$ and $-1.1 \cdot 10^{-6}$ respectively.

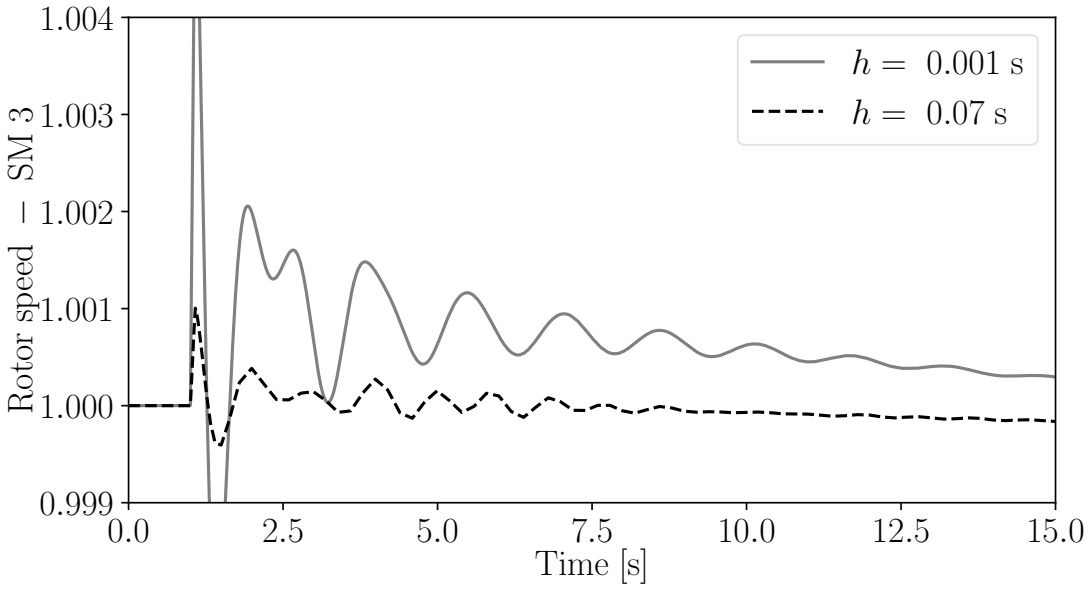

Figure 6: Delay-free system: Rotor speed of SM 3, $\theta = 0.49$.

4.2 IEEE 39-Bus System with Inclusion of Delays

We next consider the power system model with inclusion of delays. To this end, we assume that the input signals of all PSSs, as well as the frequency signal of the AGC, are impacted by a constant delay of $\tau = 60$ ms. The resulting model is small-signal stable as all finite eigenvalues lie in the open left half of the s-plane.

We examine the numerical deformation introduced by the TDI method. In particular, we begin with the TM, the small-disturbance dynamics of which are assessed by finding the eigenvalues of the matrix pencil (27) for $\theta = 0.5$. Conclusions are similar to the ones obtained for the delay-free system, i.e., the TM remains stable for realistic time step sizes, while for large steps all modes are numerically underdamped. We then study the effect of varying the parameter θ. To this end, we perform a parameter sweep over θ to determine for different step sizes the value $\theta = \theta_\zeta$ for which the damping ratio $\hat{\zeta}$ of the numerically deformed eigenvalue $\hat{s}$ closely matches the damping ratio ζ of the corresponding system eigenvalue s. The results for the pair $s_{3,4} = -0.013322 \pm j0.050422$ are shown in Table 1. For $h = 0.01$ s, the mode's

damping is most accurately captured for $\theta = 0.484$. As h increases, θ_ζ approaches 0.5. We also note that for values of h that are not integer multiples of the time step, part of the numerical deformation is due to linear interpolation, according to (10).

Table 1: System with a delay $\tau = 60$ ms: Value of θ_ζ for the pair of eigenvalues $\hat{s}_{3,4}$, for different values of h.

h [s]	0.01	0.03	0.06	0.08	0.1	0.15	0.2
θ_ζ	0.484	0.494	0.497	0.498	0.498	0.499	0.499

By increasing the value of the time delay τ from 60 ms to 100 ms, a complex pair of eigenvalues moves to the right half of the s-plane and the system becomes unstable. This is consistent with Fig. 7a, which shows for $h = 0.001$ s the time-domain response of the rotor speed of SM 8 assuming that the active power consumption of the load connected to bus 16 includes a stochastic component. The latter is modeled as stochastic normally-distributed noise, with 0 mean value and 1% standard deviation.

When we apply the TM in this case, Fig. 8a shows that with an increase of h beyond 0.01 s, the method makes the system appear stable, despite actually being unstable. This result is consistent with Fig. 7b, which indicates that for $h = 0.2$ s, the numerical method fails to capture the instability of the system. For completeness, we further check this result for the case of a large disturbance, by considering the same contingency as above, i.e., a three-phase fault at bus 6. Figure 8b shows the rotor speed of SM 8 following the contingency. The maximum and average numerical errors with (respect to a reference trajectory obtained with $h = 0.0001$ s) are, respectively, $1.9 \cdot 10^{-3}$ and $5.9 \cdot 10^{-6}$ for $h = 0.01$ s; and $1.7 \cdot 10^{-3}$ and $2.0 \cdot 10^{-5}$ for $h = 0.2$ s. The plot confirms consistency with the SSSA results for a large enough time step ($h = 0.2$ s).

We then study the effect of the θ parameter on the precision of the TDI method. To this end, we examine the numerical deformation caused by the Theta method to the two rightmost pairs of eigenvalues. We observe that for small time steps a slight variation of θ allows to capture the instability of the system. This is illustrated in Fig. 9 where, $\theta = 0.503$ leads to consistent results between SSSA of the system and the Theta method. Nevertheless, there are practical restrictions for large steps. In particular, attempting to accurately represent one mode through variation of θ may negatively impact the accuracy of another mode. This is because faster dynamics typically suffer from larger numerical distortions under the same variation of h, with the phenomenon being more prominent for large steps. An example of such a behavior is shown in Fig. 10.

4.3 Modified 39-Bus System with Inverter-Based DERs

This section presents simulation results based on a modified version of the IEEE 39-bus system, where part of the synchronous generation has been replaced by inverter-based DERs, as shown in Fig. 11. In

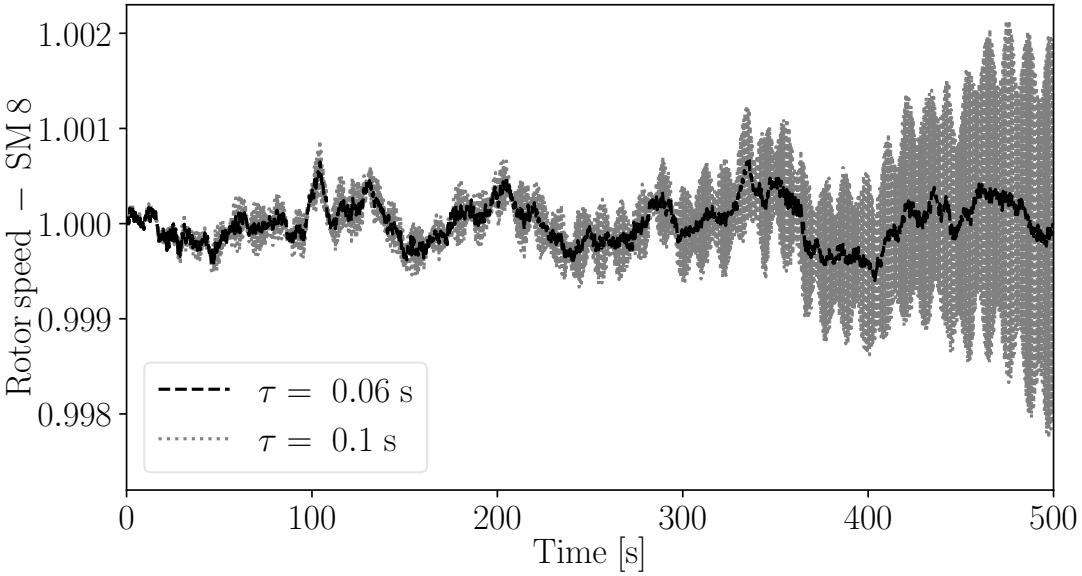

(a) Effect of increasing τ from 60 to 100 ms, $h = 0.001$ s.

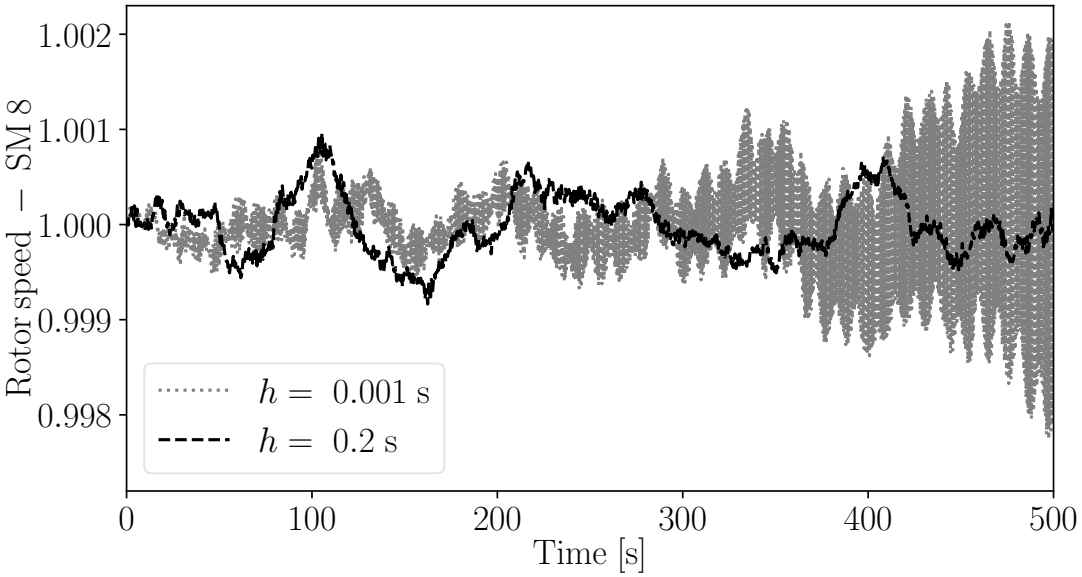

(b) Effect of increasing h from 0.001 s to 0.2 s, $\tau = 100$ ms.

Figure 7: Rotor speed of SM 8 in the presence of stochastic loads.

particular, the SMs at buses 30, 34, 35, 36 and 37 have been replaced by DERs of the same capacity. Each DER comprises an inner control loop that regulates the d and q components of the current in the dq reference frame, and two outer loops for primary frequency and voltage control, respectively [33]. The input signal of the frequency control of each DER is provided by a synchronous reference frame phase-locked loop (SRF-PLL). The control parameters of the DERs are shown in Table 2, where $\mathrm{K_P}$, $\mathrm{K_I}$ denote the gains of the corresponding PI controllers, $\mathrm{T_d}$, $\mathrm{T_q}$ are the d and q axis current controller time constants and R, $\mathrm{T_f}$, $\mathrm{T_q}$ denote the droop gain, the droop time constant and the washout filter time

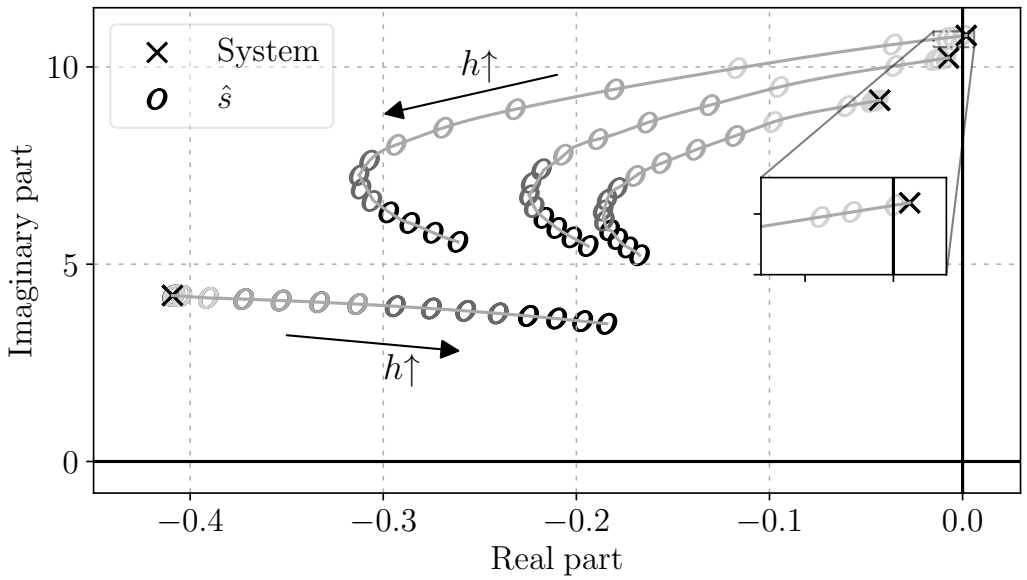

(a) Eigenvalue numerical deformation as h is varied. The system is small-signal unstable.

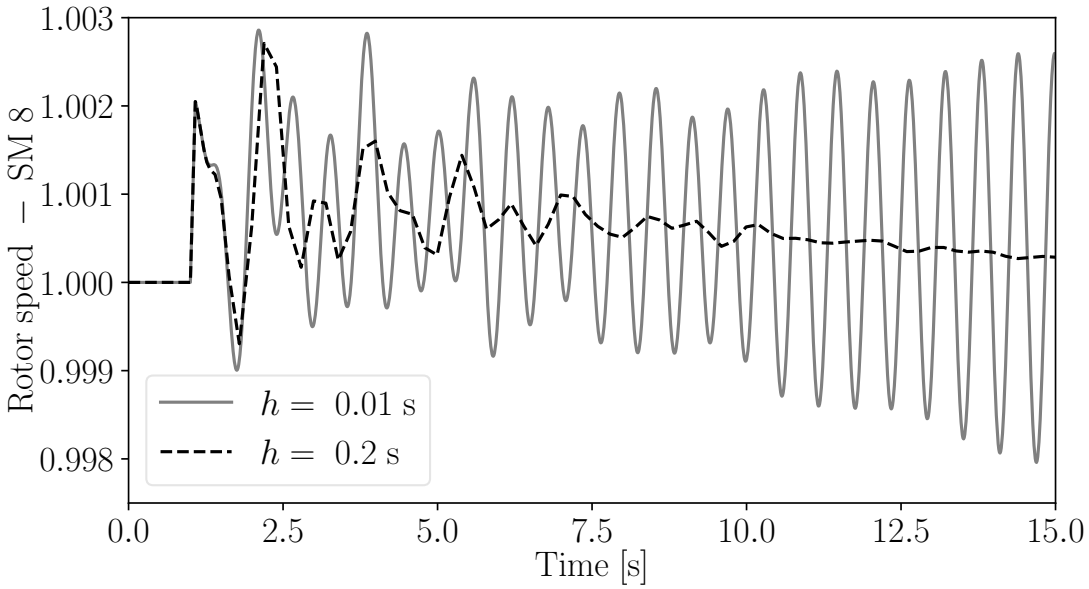

(b) Rotor speed of SM 8 following a three-phase fault.

Figure 8: System with $\tau = 100$ ms solved with TM ($\theta = 0.5$).

constant respectively.

Table 2: Parameters of DER controllers.

Controller	Parameters		
PLL	$K_P = 0.0001$	$K_I = 1$	
Current	$T_d = 0.01$ s	$T_q = 0.01$ s	
Frequency	$R = 0.1$	$T_f = 0.1$ s	$T_w = 0.1$ s
Voltage	$K_P = 10$	$K_I = 10$	

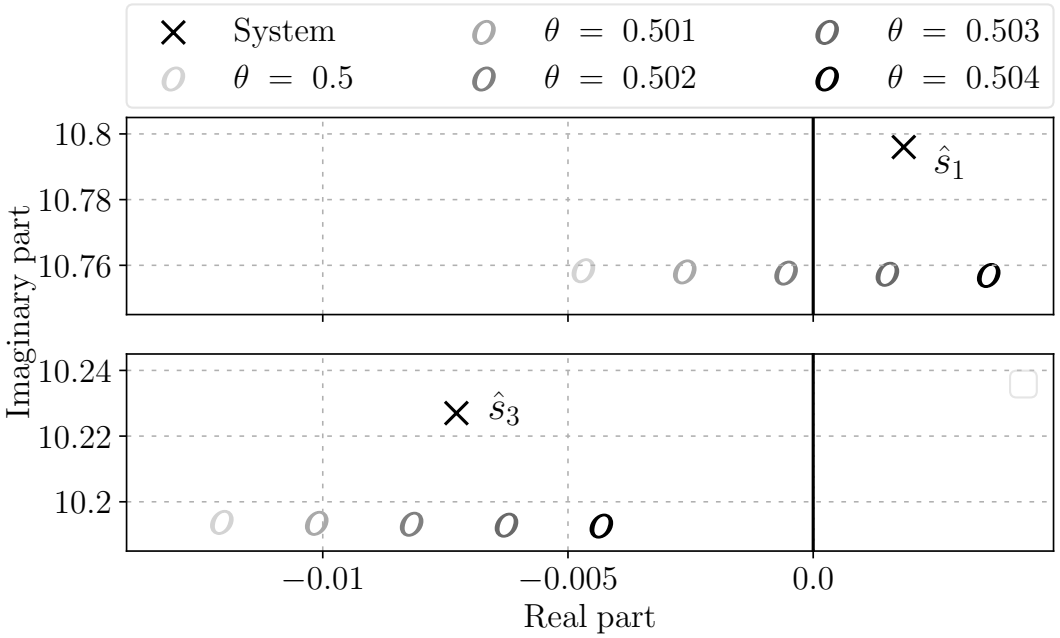

Figure 9: System with delays: Effect of θ on the numerical deformation of the two rightmost modes, $h = 0.02$ s.

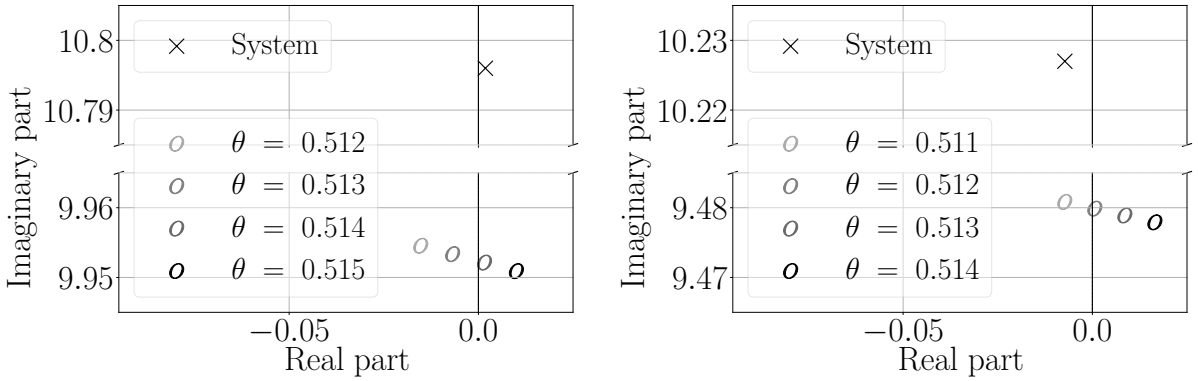

(a) $\hat{s}_1$. (b) $\hat{s}_3$.

Figure 10: System with delays: Effect of θ on the numerical deformation of the two rightmost modes, $h = 0.1$ s.

To study the impact of time delays, we assume that the measurements of the DER voltage and frequency controllers, the phase-locked loops (PLLs), the PSSs and the AGC are all impacted by a 60 ms delay. For the needs of this example, we make the PLLs oscillatory, a behavior often observed under weak-grid conditions [34]. Figure 12 depicts the rightmost eigenvalues of the modified system, as well as the corresponding numerically deformed eigenvalues produced by the TM. As it can be seen, despite the system being stable, increasing h to large enough values makes it appear unstable, as the real part of a numerically deformed eigenvalue ($\hat{s}_{\text{cr}} = -0.000711 + j19.399$) becomes positive. In other words, the TM is expected to be numerically unstable in this scenario, causing errors to grow uncontrollably.

We next study the effect of varying the magnitudes of the coefficients of delayed terms in the system's equations, on numerical stability. Results are presented in Fig. 13 and indicate that even a slight variation of 1% significantly impacts the numerical stability of the TDI method. In particular, a time step of

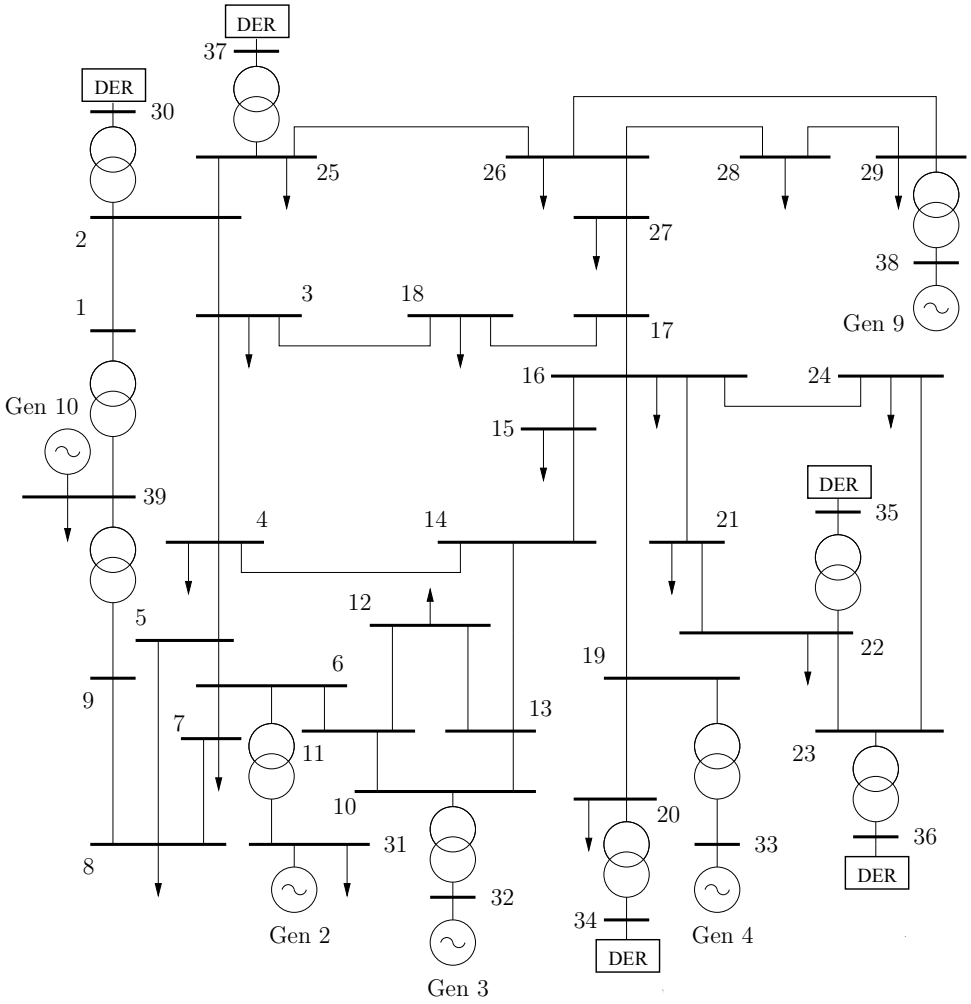

Figure 11: Modified version of 39-bus system with DERs connected to buses 30, 34, 35, 36 and 37.

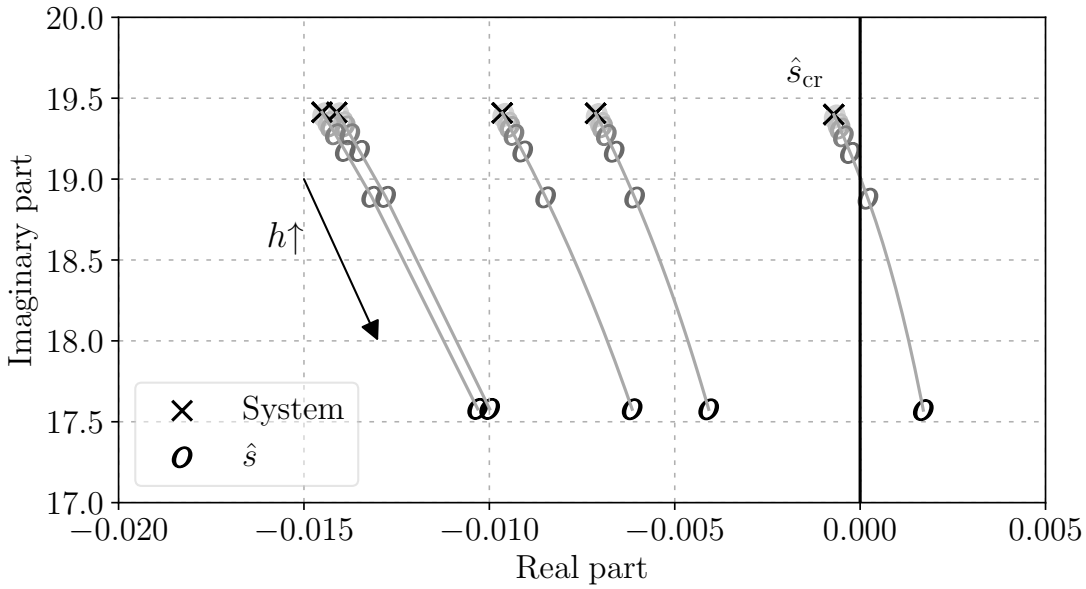

Figure 12: Modified system with delays: Numerical deformation of rightmost eigenvalues under the effect of TM.

$h = 0.02$ s is enough to destabilize the TM in this scenario.

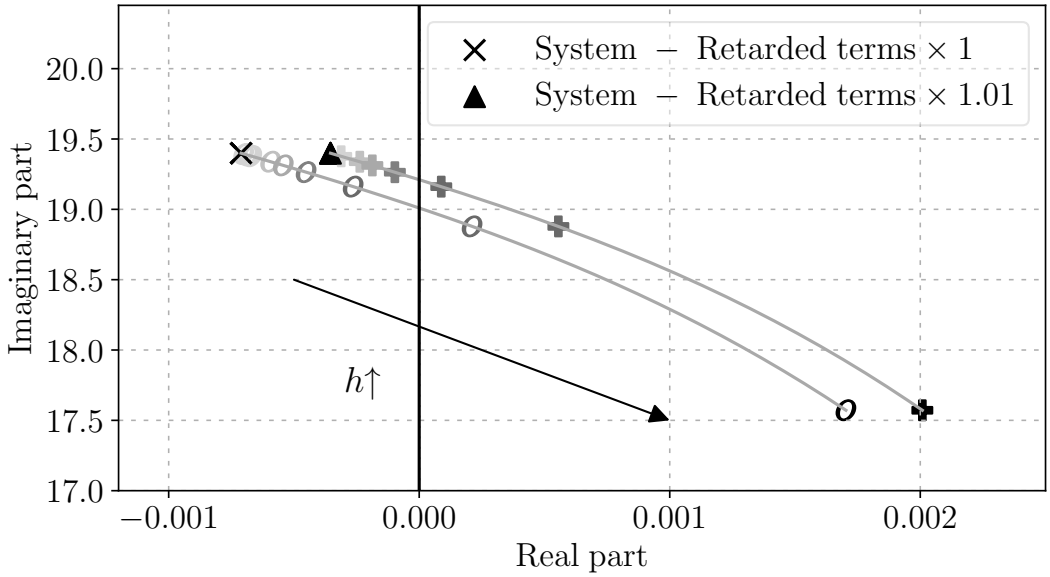

Figure 13: Modified system with delays: Numerical deformation of rightmost eigenvalues caused by increased magnitudes of coefficients of delayed variables, TM. The TM is destabilized for $h \geq 0.02$ s.

We further check the above conclusions through a TDI of the system. In particular, we consider a three-phase fault occurring at bus 6 at $t = 1$ s and cleared after 80 ms by opening the line that connects buses 5 and 6. The response of the rotor speed of SM 4 is shown in Fig. 14. For the sake of comparison, the delay-free system is also plotted in the same figure. Figure 14b confirms that for a large enough time step (in this case 0.2 s), the TM makes an otherwise stable trajectory of the system appear unstable. The maximum and average numerical errors are $5.6 \cdot 10^{-5}$ and $-4.4 \cdot 10^{-7}$ for $h = 0.001$ s; and $7.6 \cdot 10^{-4}$ and $8.6 \cdot 10^{-6}$ for $h = 0.2$ s.

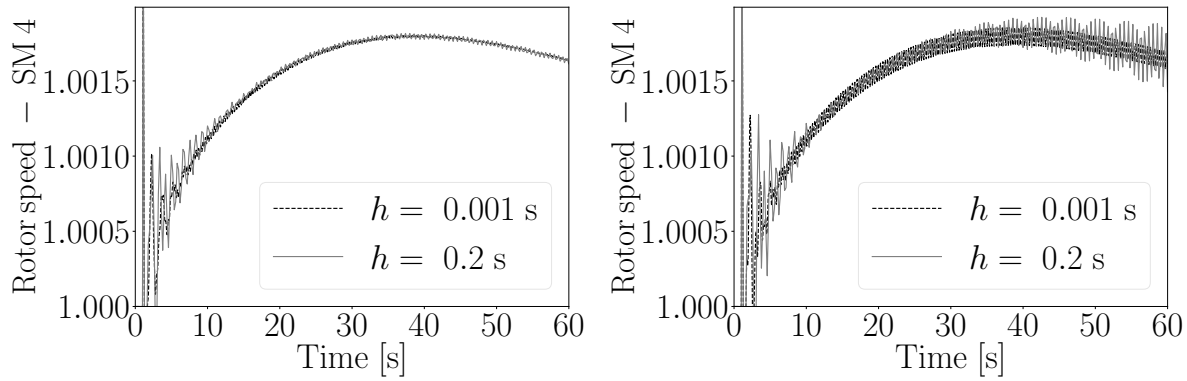

(a) Without delays.

(b) With delays.

Figure 14: Modified system with delays: Rotor speed of SM 4 for $\theta = 0.5$ (TM) following a three-phase fault at bus 6.

Up to this point, all examples are based on the Theta method, which is the one chosen to showcase the extent of numerical deformation in the presence of time delays in power systems. Nevertheless, spe-

cialized methods are reported that can achieve superior accuracy for time-delayed systems [22]. Figure 15 compares the performance of the TM and the 2-stage Radau IIA method for the rightmost eigenvalue $\hat{s}_{cr}$ of Fig. 12. Figures 15b and 15c show that for the same values of h that destabilize the TM, Radau IIA retains numerical stability and also mitigates numerical deformation in terms of relative error [2]. However, unlike the TM, Radau IIA overdamps $\hat{s}_{cr}$, increasing the numerically deformed eigenvalue's damping ratio ζ (Fig. 15d).

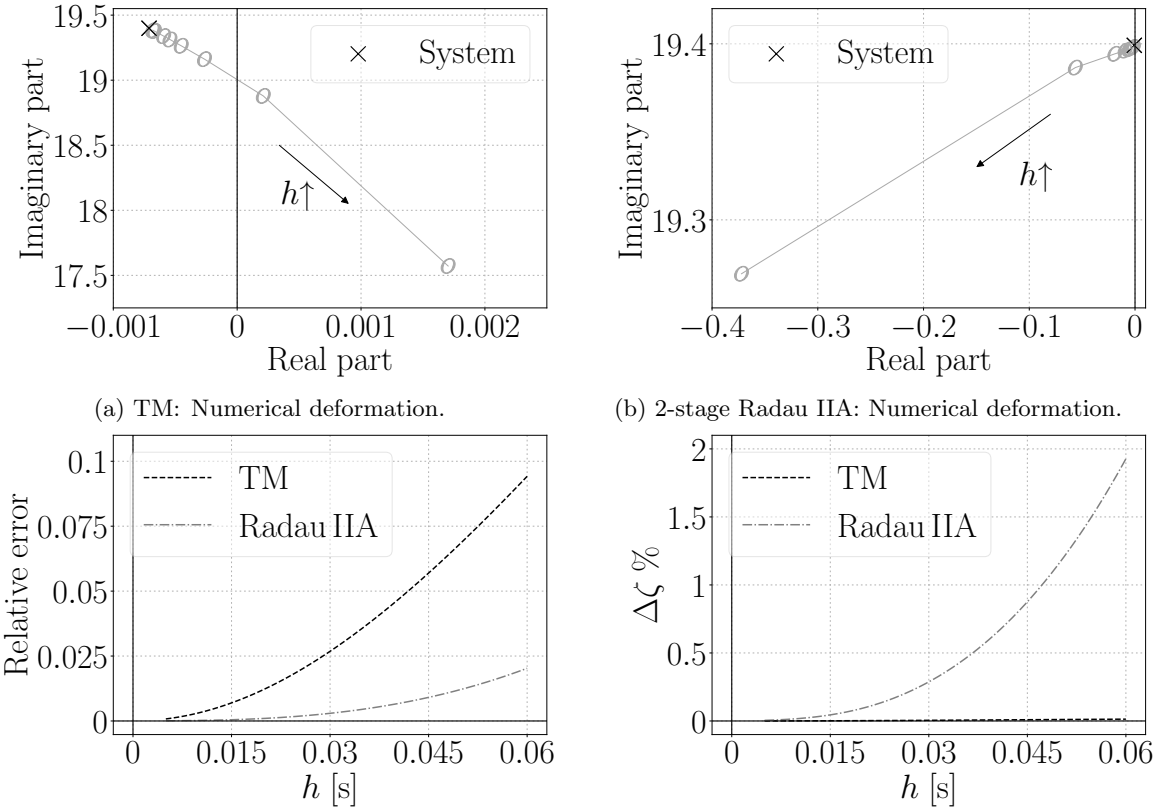

(a) TM: Numerical deformation.

(b) 2-stage Radau IIA: Numerical deformation.

(c) Relative error.

(d) Damping ratio error.

Figure 15: Modified system with delays: Numerical deformation of $\hat{s}_{cr}$ caused by different TDI methods.

We finally examine how the θ parameter can be employed to compensate for the numerical deformation introduced by the Theta method in this scenario. In particular, θ is altered to a value $\theta_\zeta < 0.5$ for which $\hat{s}_{\text{cr}}$ has the same damping ζ_{cr} as s_{cr}, i.e. $\hat{\zeta} = \zeta_{\text{cr}}$. In Fig. 16a it is shown that θ needs to be slightly modified by about 10^{-5} for $h = 0.03$ s and by about $1.5 \cdot 10^{-5}$ for $h = 60$ ms. A time-domain simulation of the system further confirms this conclusion, see Fig. 16b.

4.4 All-Island Irish Transmission System with Delays

This section includes simulation results based on a 1,502-bus dynamic model of the AIITS. The delay-free model of the system has in total $1,629$ states and $9,897$ algebraic variables. The resulting pencil's dimensions are $11,526 \times 11,526$. Application of the matrix pencil method – even in the case where

[2] Euclidean distance of s and $\hat{s}$ in the complex plain divided by the magnitude of s.

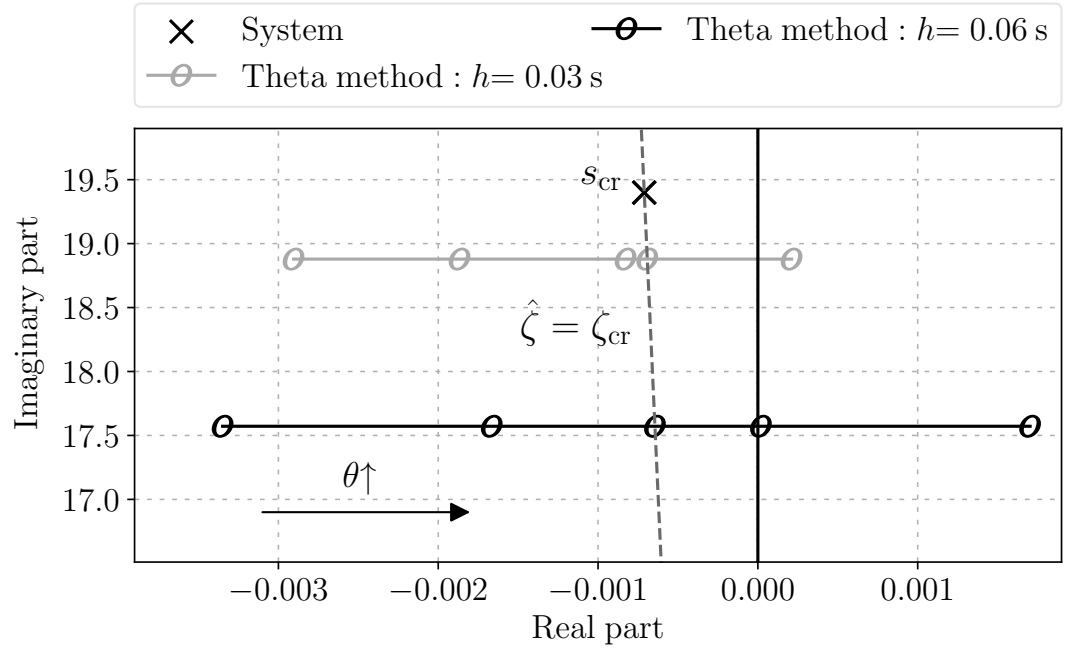

(a) Effect of a very small variation of θ from 0.4997 to 0.5.

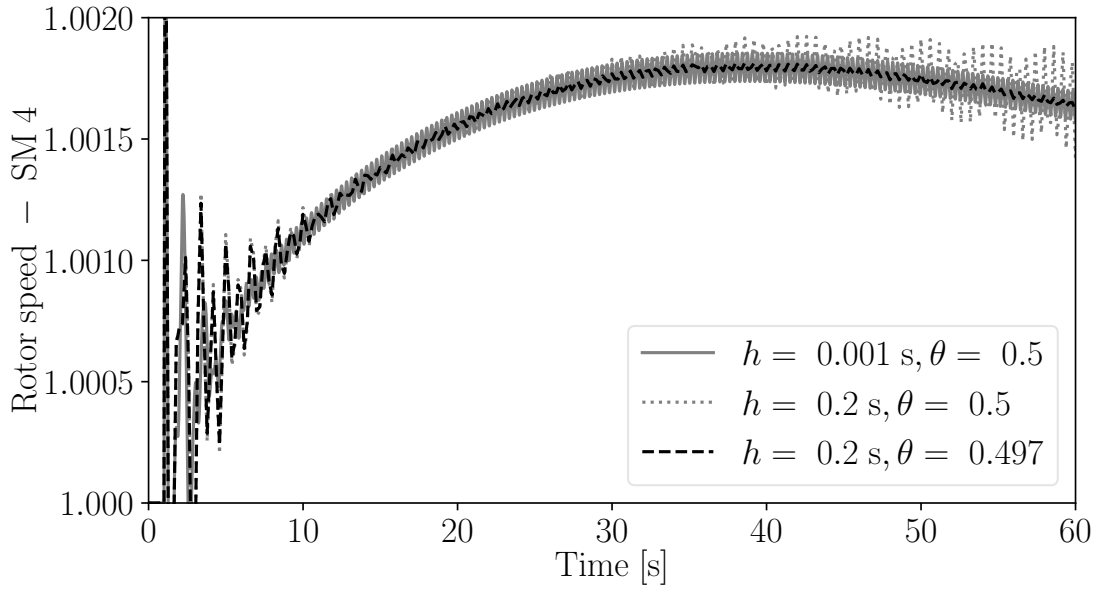

(b) Rotor speed of SM 4 following a three-phase fault at bus 6.

Figure 16: Modified system with delays: Effect of varying θ on the precision of the Theta method.

the system is impacted by a single delay – produces a pencil in the form of (27) with dimensions over $23,000 \times 23,000$. This size makes the use of standard methods, like QR/QZ factorization, impractical. Hence, for the eigenvalue analysis we consider instead the equivalent delay-differential equation problem, as in [12, 26], which consists of $1,629$ state variables.

We consider 28 delayed variables in total, impacting the voltage and the frequency measurements of the system's AVRs and PSSs respectively, with the delay magnitude being constant and equal to 100 ms. Therefore, when choosing the time step of the Theta method to be equal to τ, i.e., $h = 100$ ms, the

dimensions of (26) double. In the same way, considering $h = 50$ ms makes the dimensions $4,887 \times 4,887$, three times the original size of the system. Simulations in this section are executed using a computer with a 13th Gen Intel(R) Xeon(R) Gold 5416S, 2.0 GHz (up to 3.8 GHz turbo) processor, 384 GB of RAM, and running a 64-bit Linux OS.

The induced numerical deformation for the aforementioned cases is depicted in Fig. 17, in the case of the TM. The computational time for $h = 100$ and $h = 50$ ms is approximately 4 m 20 s and 12 m

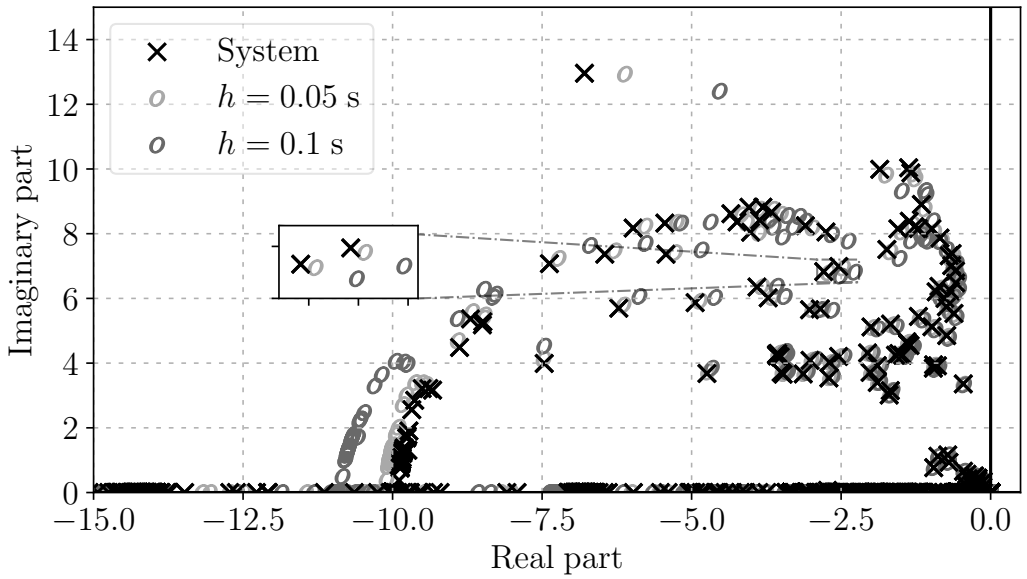

Figure 17: AIITS: Numerical deformation of rightmost eigenvalues under the effect of TM.

19 s respectively. Further reducing the TDI method's step size or considering multiple time delays would increase the dimensions of the system to values close or over $10,000$. The latter constitutes an empirical limit for performing QR factorization, the standard approach for calculating the whole spectrum of a system. Nevertheless, the matrix pencil approach can be applied to larger scale system and offer insight on the induced numerical deformation, under certain assumptions.

We finally examine the impact of h in the computational time and the error of TDI simulations. To this end we conduct a 30 s simulation of the AIITS when the constant power load of bus 704 is disconnected at $t = 1$ s. We monitor the total computational time and the average error of the frequency of the SM which is connected to bus $1,146$. The trajectory calculated for $h = 1$ ms is set as reference. Results presented in Figures 18a and 18b respectively illustrate the dependence of computational time and average error on the chosen time step.

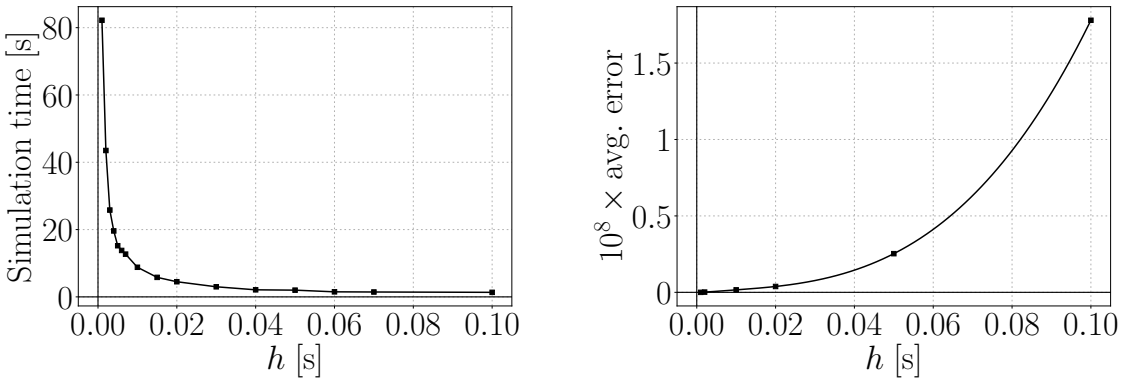

(a) Simulation time.

(b) Average error

Figure 18: AIITS: computational time and error of the TM for 30 of simulation time.

5 Conclusions

The paper shows that standard implicit TDI methods, such as the trapezoidal and Theta method, can become numerically unstable when applied to power system models impacted by multiple time-delayed variables. This is shown to arise from the combined effect of a large number of delayed variables and large Jacobian coefficients. Interestingly, the role of the delay magnitudes themselves in numerical instability is relatively minor. The mechanism behind this numerical phenomenon is first shown for a linear test delay differential equation. Subsequently, a systematic analysis that accounts for the dynamics of real-world power system models is carried out through a unified numerical stability and accuracy analysis based on SSSA. Theoretical findings of the paper are supported by simulation results conducted based on the IEEE 39-bus system and scalability is evaluated through simulations on a real-world size model of the Irish transmission system. The main limitation of the proposed analysis approach, i.e., its small-signal nature, is also duly discussed.

The findings of this work have relevant practical applications. Specifically, they can be employed to internally check numerical stability and accuracy of a given integration method within the time-domain simulation routines of modern power system software. The proposed matrix pencil approach, in contrast with standard analysis techniques, provides insight into the dynamics of the system and predicts numerical instabilities. Thus it enables the selection of an appropriate time step size to meet prescribed simulation accuracy criteria while accounting for the numerical deformation of the system's dynamics introduced by the integration method. Naturally, reducing the time step size enhances accuracy but increases computational cost. Additionally, these findings can aid in comparing alternative TDI methods to achieve accurate and stable simulations without requiring a substantial reduction in time step size.

Future work will focus on the effect of adaptive step-size algorithms, as well as on comparisons with the performance of specialized TDI methods for delay differential equations, such as the family of Radau IIA methods. Moreover, a promising direction for future work is studying the effects of more

general scenarios involving stochastic and event-driven delays.

Appendix A Derivation of (4)

Applying the Laplace transform $\mathcal{L}\{\cdot\}$ to (2) and omitting for simplicity the initial conditions:

$$\begin{aligned} s\mathcal{L}\{\boldsymbol{x}\} &= \mathcal{L}\{\boldsymbol{f}(\boldsymbol{x},\boldsymbol{y})\}\,, \\ \mathbf{0}_{\mu,1} &= \mathcal{L}\{\boldsymbol{g}(\boldsymbol{x},\boldsymbol{y})\}\,. \end{aligned} \tag{A.1}$$

Using (3) and (5), we obtain:

$$\begin{aligned} (z-1)\mathcal{Z}\{\boldsymbol{x}_n\} &= h(\theta+(1-\theta)z)\mathcal{Z}\{\boldsymbol{f}(\boldsymbol{x}_n,\boldsymbol{y}_n)\}\,, \\ \mathbf{0}_{\mu,1} &= \mathcal{Z}\{\boldsymbol{g}(\boldsymbol{x}_{n+1},\boldsymbol{y}_{n+1}\}\,, \end{aligned} \tag{A.2}$$

where $\mathcal{Z}\{\cdot\}$ denotes the Z-transform. By applying the inverse Z-transform to (A.2), we arrive to (4).

Appendix B Proof of (26)

The proof of (26) goes as follows:

Proof. Let us rewrite (25) as follows:

$$\mathbf{E}\mathbf{x}_{n+1} = \mathbf{D}_0\mathbf{x}_n + \mathbf{D}_1\mathbf{x}_{n-1} + \ldots + \mathbf{D}_r\mathbf{x}_{n-r}\,,$$

where $\mathbf{D}_0 = \mathbf{A}+\mathbf{B}_0$, $\mathbf{D}_j = \mathbf{B}_j + \mathbf{C}_j$, $j = 1,2,\ldots,r-1$, and $\mathbf{D}_r = \mathbf{C}_r$. Then, by setting:

$$\boldsymbol{\psi}_{n+1}^{[i]} = \mathbf{x}_{n+1-i}\,, \qquad \boldsymbol{\psi}_{n}^{[i]} = \mathbf{x}_{n-i}\,,$$

where $i = 0,1,2,\ldots,r$, we have equivalently:

$$\mathbf{M}\boldsymbol{\psi}_{n+1}^{[0]} = \mathbf{D}_0\boldsymbol{\psi}_{n+1}^{[1]} + \mathbf{D}_1\boldsymbol{\psi}_{n+1}^{[2]} + \ldots + \mathbf{D}_{r-1}\boldsymbol{\psi}_{n+1}^{[r]} + \mathbf{D}_r\boldsymbol{\psi}_{n}^{[r]}\,,$$

which can be then expressed in the form of (26), where $\boldsymbol{\psi}_n = (\boldsymbol{\psi}_n^{[0]}, \boldsymbol{\psi}_n^{[1]}, \ldots, \boldsymbol{\psi}_n^{[r]})$, and:

$$\mathbf{F} = \begin{bmatrix} \mathbf{0}_{rq\times q} & \boldsymbol{I}_{rq\times rq} \\ \mathbf{M} & -\mathbf{D} \end{bmatrix},\ \mathbf{G} = \begin{bmatrix} \boldsymbol{I}_{rq\times rq} & \mathbf{0}_{rq\times q} \\ \mathbf{0}_{q\times rq} & \mathbf{D}_r \end{bmatrix},$$
$$\mathbf{D} = [\mathbf{D}_0\ \mathbf{D}_1\ \ldots\ \mathbf{D}_{r-1}]\,.$$

where $q = \nu + \mu$.

□

References

[1] C. Guo, J. Zhang, S. Yang, and N. Lv, "Impact of time delay on the control link in small signal dynamics of LCC-HVDC system," *IEEE Transactions on Power Delivery*, vol. 38, no. 5, pp. 3342–3355, 2023.

[2] Y. Dong, K. Sun, J. Wang, S. Wang, H. Huang, T. Liu, and Y. Liu, "A time-delay correction control strategy for HVDC frequency regulation service," *CSEE Journal of Power and Energy Systems*, pp. 1–11, 2022.

[3] W. Yao, Y. Wang, Y. Xu, and C. Dong, "Small-signal stability analysis and lead-lag compensation control for dc networked-microgrid under multiple time delays," *IEEE Transactions on Power Systems*, vol. 38, no. 1, pp. 921–933, 2023.

[4] M. Liu, I. Dassios, G. Tzounas, and F. Milano, "Stability analysis of power systems with inclusion of realistic-modeling WAMS delays," *IEEE Transactions on Power Systems*, vol. 34, no. 1, pp. 627–636, 2018.

[5] G. S. Ledva, E. Vrettos, S. Mastellone, G. Andersson, and J. L. Mathieu, "Managing communication delays and model error in demand response for frequency regulation," *IEEE Transactions on Power Systems*, vol. 33, no. 2, pp. 1299–1308, 2018.

[6] L. Jin, C.-K. Zhang, Y. He, L. Jiang, and M. Wu, "Delay-dependent stability analysis of multi-area load frequency control with enhanced accuracy and computation efficiency," *IEEE Transactions on Power Systems*, vol. 34, no. 5, pp. 3687–3696, 2019.

[7] G. Tzounas, R. Sipahi, and F. Milano, "Damping power system electromechanical oscillations using time delays," *IEEE Transactions on Circuits and Systems I: Regular Papers*, vol. 68, no. 6, pp. 2725–2735, 2021.

[8] P. Kundur, *Power System Stability and Control*. New York: Mc-Grall Hill, 1994.

[9] S. Tripathy and N. Rao, "A-stable numerical integration method for transmission system transients," *IEEE Transactions on Power Apparatus and Systems*, vol. 96, no. 4, pp. 1399–1407, 1977.

[10] J. Sanchez-Gasca, R. D'Aquila, W. Price, and J. Paserba, "Variable time step, implicit integration for extended-term power system dynamic simulation," in *Proceedings of Power Industry Computer Applications Conference*, 1995, pp. 183–189.

[11] DIgSILENT Power System Solutions, "DIgSILENT PowerFactory," 2025, digsilent.de/powerfactory, Accessed: 30-09-2025.

[12] F. Milano and M. Anghel, "Impact of time delays on power system stability," *IEEE Transactions on Circuits and Systems I: Regular Papers*, vol. 59, no. 4, pp. 889–900, 2011.

[13] I. Hiskens, "Time-delay modelling for multi-layer power systems," in *Proceedings of the 2003 International Symposium on Circuits and Systems, 2003. ISCAS '03.*, vol. 3, 2003, pp. III–III.

[14] K. Engelborghs and D. Roose, "On stability of LMS methods and characteristic roots of delay differential equations," *SIAM Journal on Numerical Analysis*, vol. 40, no. 2, pp. 629–650, 2002.

[15] X. Hu, Y. Cong, and G.-D. Hu, "Delay-dependent stability of linear multistep methods for DAEs with multiple delays," *Numerical Algorithms*, vol. 79, no. 3, pp. 719–739, 2018.

[16] A. Bellen and M. Zennaro, *Numerical Methods for Delay Differential Equations.* Oxford, UK: Oxford Science Publications, 2003.

[17] N. Guglielmi and E. Hairer, "Implementing Radau IIA methods for stiff delay differential equations," *Computing (Vienna/New York)*, vol. 67, no. 1, p. 1 – 12, 2001.

[18] T. Koto, "Stability of implicit-explicit linear multistep methods for ordinary and delay differential equations," *Frontiers of Mathematics in China*, vol. 4, no. 1, pp. 113–129, 2009.

[19] E. Hairer and G. Wanner, *Solving Ordinary Differential Equations II: Stiff and Differential-Algebraic Problems.* New York: Springer-Verlag, 1991.

[20] G. Tzounas, I. Dassios, and F. Milano, "Small-signal stability analysis of numerical integration methods," *IEEE Transactions on Power Systems*, vol. 37, no. 6, pp. 4796–4806, 2022.

[21] C. Tajoli, G. Tzounas, and G. Hug, "Mode-shape deformation of power system DAEs by time-domain integration methods," in *2023 IEEE Belgrade PowerTech*, 2023, pp. 1–6.

[22] G. Tzounas, I. Dassios, and F. Milano, "Small-signal stability analysis of implicit integration methods for power systems with delays," *Electric Power Systems Research*, vol. 211, p. 108266, 2022.

[23] S. Campbell and L. Petzold, "Differential-algebraic equations," *Scholarpedia*, vol. 3, p. 2849, 2008.

[24] R. März, "Numerical methods for differential algebraic equations," *Acta Numerica*, vol. 1, p. 141–198, 1992.

[25] S. Campbell and C. W. Gear, "The index of general nonlinear DAEs," *Numerische Mathematik*, vol. 72, no. 2, pp. 173–196, 1995.

[26] F. Milano, I. Dassios, M. Liu, and G. Tzounas, *Eigenvalue Problems in Power Systems*. CRC Press, Taylor & Francis Group, 2020.

[27] C. Li, Y. Chen, T. Ding, Z. Du, and F. Li, "A sparse and low-order implementation for discretization-based eigen-analysis of power systems with time-delays," *IEEE Transactions on Power Systems*, vol. 34, no. 6, pp. 5091–5094, 2019.

[28] J. H. Chow, *Power System Coherency and Model Reduction*, ser. Power Electronics and Power Systems 94. New York: Springer-Verlag, 2013.

[29] G. C. Verghese, I. J. Pérez-Arriaga, and F. C. Schweppe, "Selective modal analysis with applications to electric power systems, part ii: the dynamic stability problem," *IEEE Transactions on Power Apparatus and Systems*, vol. PAS-101, no. 9, pp. 3126–3134, 1982.

[30] Illinois Center for a Smarter Electric Grid (ICSEG), "IEEE 39-Bus System," publish.illinois.edu/smartergrid/ieee-39-bus-system/, Accessed: 30-09-2025.

[31] F. Milano, *Power System Modelling and Scripting*. Springer, 2010.

[32] F. Milano, "A Python-based software tool for power system analysis," in *Proceedings of the IEEE PES General Meeting*, 2013.

[33] Álvaro Ortega and F. Milano, "Frequency control of distributed energy resources in distribution networks," *IFAC-PapersOnLine*, vol. 51, no. 28, pp. 37–42, 2018, 10th IFAC Symposium on Control of Power and Energy Systems CPES 2018.

[34] R. Ávila Martínez, L. Rouco, J. García-Aguilar, J. Renedo, and L. Sigrist, "Impact of PLL control on small-signal stability of wind DFIGs," in *Proceedings of the IEEE PES General Meeting*, 2020, pp. 1–5.